

**Exclusion processes on a roundabout traffic model with constrained resources**Ankita Gupta  and Arvind Kumar Gupta \**Department of Mathematics, Indian Institute of Technology Ropar, Rupnagar-140001, Punjab, India*

(Received 19 June 2023; accepted 16 November 2023; published 8 December 2023)

Motivated by the vehicular traffic phenomenon at roundabouts, we examine how the limited availability of resources affects the movement of two distinct types of particles on bidirectional lanes connected by two bridges, with each bridge specifically designated for the transportation of one species. To provide a theoretical ground for our findings, we employ a mean-field framework and successfully validate them through dynamic Monte Carlo simulations. Based on the theoretical analysis, we analytically derive various stationary properties, such as the particle densities, phase boundaries, and particle currents, for all the possible symmetric as well as asymmetric phases. The qualitative as well as quantitative behavior of the system is significantly affected by the constraint on the number of resources. The complexity of the phase diagram shows a nonmonotonic behavior with an increasing number of particles in the system. Analytical arguments enable the identification of several critical values for the total number of particles, leading to a qualitative change in the phase diagrams. The interplay of the finite resources and the bidirectional transport yields unanticipated and unusual features such as back-and-forth transition, the presence of two congested phases where particle movement is halted, as well as shock phases induced by boundaries and the bulk of the system. Also, it is found that spontaneous symmetry-breaking phenomena are induced even for very few particles in the system. Moreover, we thoroughly examine the location of shocks by varying the parameters controlling the system's boundaries, providing insights into possible phase transitions.

DOI: [10.1103/PhysRevE.108.064116](https://doi.org/10.1103/PhysRevE.108.064116)**I. INTRODUCTION**

Traffic problem poses a pervasive challenge in urban areas across the globe, resulting in noteworthy economic, environmental, and social consequences [1]. The central emphasis of numerous researchers lies in strategizing, designing, and executing transportation networks and traffic control systems to promote the seamless and effective movement of transportation and services. Statistical physicists have made valuable contributions to the field of traffic science by creating traffic models and deriving overarching insights about the fundamental principles that govern traffic phenomena. One of the simplest nonequilibrium models that is often employed to study traffic flow and congestion is the totally asymmetric simple exclusion process (TASEP) [2–6]. This model provides insights into the collective behavior of particles, analogous to vehicles in traffic, and can help in understanding and developing strategies to mitigate traffic congestion. TASEPs have proven to be effective in studying the dynamics of various processes, including biopolymerization kinetics [7], protein synthesis [8–10], molecular transport through nanopores and channels [11], the movement of motor proteins along cytoskeleton filaments [12,13], and the analysis of car traffic processes [14,15], etc. Incorporating suitable boundary conditions, the model exhibits the capability to elucidate various counterintuitive phenomena such as shock formation, spontaneous symmetry breaking, phase separation, etc. [16–21].

Over the past few decades, researchers have focused their efforts on broadening the range of TASEP from its original single-species particle models to more complex multispecies bidirectional models, which showcase captivating occurrences of spontaneous symmetry breaking (SSB) [16,22]. Bidirectional transport phenomena have been observed at almost all levels, ranging from man-made structures such as vehicular motion on road networks [14] or pedestrian movement [23], to natural structures such as movement of dynein and kinesin motors along microtubule [24]. Spontaneous symmetry breaking refers to a phenomenon where a system initially exhibiting symmetrical conditions undergoes a transition to an asymmetric state without any external perturbations. The bridge model stands out as the first model that exemplifies spontaneous symmetry breaking in a bidirectional transport system, despite being subject to symmetrical conditions for both the particle species [25]. Numerous generalizations of multispecies models have been developed including Langmuir kinetics, restriction on the available resources, multiple lanes, junctions, etc. [19,26–34]. Nevertheless, the exact nature of this phenomenon and the mechanism underlying the transition to the symmetry-broken state remain topics of ongoing discussion.

Networks play a vital role in the realm of traffic flow, allowing for a deep understanding and effective management of the complex interactions and dynamics among diverse transportation components. The rising traffic demands have led to a significant expansion in the construction of new roads and the improvement of existing ones. An essential feature of these road networks is the creation of numerous points

\*akgupta@iitrpr.ac.in

where different roads meet and cross paths with one another. In past decades, different topologies of networks have been modelled and analyzed to enhance traffic flow optimization, encompassing various aspects like movement at junctions, roundabouts, shortcuts, crossroads, traffic circles, multiple lanes, etc. [15,27,31,33,35–42]. A variant investigates the stationary behaviours of a one-dimensional lane inserted with a double chain section in between [36,43–45]. In other words, a single-lane road acts as a feeder segment for two diverging branches that subsequently merge back into a single lane. In this model, the unidirectional movement of particles is considered and the dynamics of the system are strongly characterized by the entrance rate of particles to the first single lane and the exit rate from the second single lane. The presence of junctions in traffic flows enhances the efficient movement of all the traffic participants. In biological systems, microtubules form an intricate network within cells, serving as structural elements and providing pathways for intracellular transport. Motor proteins such as dynein and kinesin utilize these filaments as a transportation route, traversing along them bidirectionally and towing their cargo over substantial distances. These large networks of microtubules constitute of junctions leading to various diseases as a consequence of motor protein crowding [46,47].

An extensive research has been conducted utilizing the exclusion process to model network systems focusing on the dynamics that assume either infinite resources or are unidirectional [16,20,22,27,32,33,45]. However, many physical and biological systems, such as protein synthesis, movement of motor proteins, parking garage problems, and vehicular traffic [48–50] involve competition for limited resources. As a result, various variants have emerged, where the entrance rate of the particles is regulated based on reservoir occupancy [33,34,48,51,52], that leads to traffic jamlike situations on lanes.

Given the significance of junctions and bidirectional flow in various natural and man-made systems, we explore a modified version of the double chain section model where two distinct species of particles travel in opposite directions. Simultaneously, a global constraint on the total number of particles in the system is considered. Our aim is to explore the novel phase transitions and nontrivial impact of the limited particle resources on the phase plane. We exploit the idea of defining effective entrance-exit rates through each lane and the domain wall theory, to obtain explicit expressions for the density profiles and determine the parameter range for which we expect congestion and symmetry breaking. We analyze how the choice of the boundary rates of the particles along with the number of resources available, controls the dynamics of the system. In addition, we present a comprehensive analysis by considering suitable limiting cases to gain insights into the steady-state behavior of the system. Precisely, the dynamics of our system encourages us to answer the following questions: (i) How does the number of available particles regulate the overall dynamics of the system? (ii) Does the mean-field framework possess sufficient competence to analyze the stationary properties, such as phase diagrams and potential phase transitions? (iii) How does the presence of two bridges in the middle affect both the qualitative and quantitative changes in the complexity of the phase diagram?

## II. MODEL

To understand the bidirectional movement observed in various driven diffusive systems passing through roundabouts, we present an open system that employs an exclusion process (TASEP) and incorporates two distinct types of particles in a constrained environment. Specifically, the setup comprises of two distinct lanes, denoted as P and Q, which facilitate the movement of particles in both directions. These lanes are connected by bridges, namely  $B_+$  and  $B_-$ , as clearly illustrated in Fig. 1. The two species of particle moving in opposite directions are represented as (+) and (−). Lane P acts as an input/output lane for the (+)/(−) species while lane Q acts as an output/input lane for the (+)/(−) species. The bridge lane  $B_+$  accommodates the (+) species, whereas  $B_-$  caters to the (−) species. Each lane is composed of fixed  $N$  sites identified as  $i \in \{1, 2, \dots, N\}$  (Fig. 1). The sites  $i = 1$  and  $i = N$  describe the left and right boundary whereas the rest  $N - 2$  constitutes the bulk of each lane. The hard-core exclusion principle is enforced to prevent more than one particle from occupying a specific site at the same time, which mimics the physical constraints of various transport systems. The sites  $i = 1$  of lane P and the site  $i = N$  of lane Q are connected to a finite pool containing  $N_p(t)$  identical particles. The total number of particles ( $N_{\text{tot}}$ ) in the system remains constant and does not vary at any given moment in time. Moreover, the pool is considered large enough to accommodate all the particles present in the system. The following transition rules govern the behavior of the particles in each lane, which are also described in Fig. 1.

(1) (+) particle: A positive particle is allowed to enter from the pool to the lane P through the left boundary ( $i = 1$ ) with rate  $\alpha^*$ , provided this site is empty, i.e., neither occupied by (+) particle nor (−) particle. In the bulk, this particle can jump at a unit rate to the adjacent site if the target site is unoccupied. If a positive particle encounters a negative particle on the adjacent site, then they swap their positions with unit rate. As soon as this particle reaches the last site ( $i = N$ ), it exits lane P to enter the first site of lane  $B_+$  with the unit rate provided it is empty.

Then, a (+) particle continues its movement along the bridge lane  $B_+$  from left to right following the hard-core exclusion principle. On reaching the right boundary of lane  $B_+$ , it has a tendency to hop onto the first site of lane Q with unit rate, provided the latter site is free from particles of both kinds.

In lane Q, this particle jumps along the bulk to the neighboring site if empty with unit rate. If the next site contains a (−) particle, then the two species exchange their positions with unit rate. A (+) particle finally escapes through the site  $i = N$  of lane Q with the rate  $\beta$  to reenter the pool.

(2) (−) particle: A particle species of this kind follows similar dynamic rules as that of positive species but in the opposite direction, i.e., from right to left. However, here, the bridge  $B_-$  is utilized instead of  $B_+$ .

It's important to note that we have made the assumption that the rates for both the forward hopping and the exchange of positions are equal for the two different types of particles. Moreover, all the lanes in the system are considered to be of identical length.

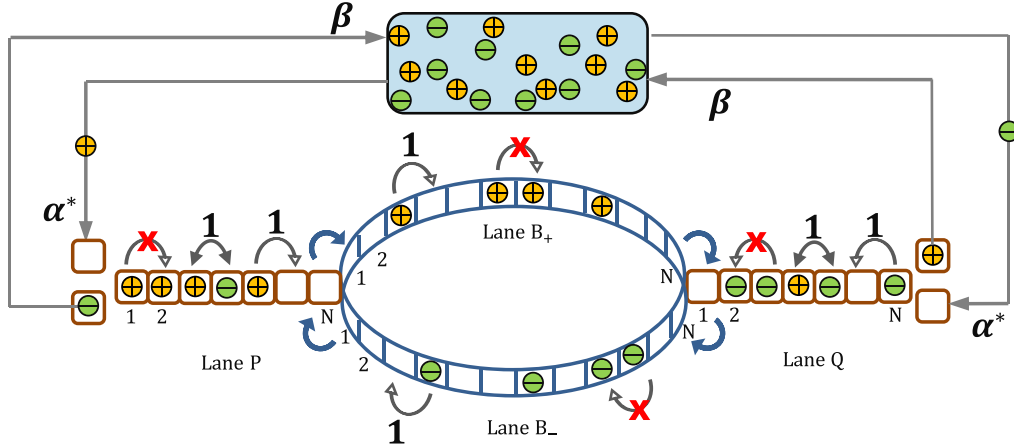


FIG. 1. Model depiction in a diagrammatic form. Arrows indicate transitions that are permitted. Prohibited transitions are indicated by red crossed arrows. The two distinct species of particles progressing from left to right and right to left are represented by (+) and (-) symbols, respectively.

The entrance rates for the particles of both kinds, denoted by  $\alpha^*$ , are controlled by the occupancy of the pool. For the sake of simplicity, we have assumed these arrival rates to be the same. To incorporate the effects of finite occupancy of the pool, we define the effective entrance rate  $\alpha^*$  as

$$\alpha^*(N_p(t)) = \alpha f(N_p(t)), \quad (1)$$

where  $\alpha$  is the entry rate in case of limited resources and  $f$  is a rate function controlling the entrance of the particles. This function  $f(N_p(t))$  must satisfy three basic conditions: (i)  $f(0) = 0$ , (ii)  $f(N_p(t))$  must be a monotonically increasing function of  $N_p(t)$ , and (iii)  $f(\infty) = 1$ . The first condition is self-evident and requires no elaboration. The second condition can be explained as follows: An increase in the pool content will result in greater flux of particles onto the lanes, so it is reasonable to define  $f$  as an increasing function of  $N_p(t)$ . The third condition serves as a connection between the situations of finite resources and an unlimited supply of particles. To proceed further, we opt for the selection of  $f$  [51] as

$$f(N_p) = N_p/N_{\text{tot}} \quad (2)$$

due to analytical amenability. When  $N_p(t) \ll N_{\text{tot}}$ , it indicates a scarcity of supply of particles onto the lanes from the pool. In case,  $N_{\text{tot}} \rightarrow \infty$ , the situation of infinite particles is recovered and thus  $N_p(t) \approx N_{\text{tot}}$  implying that  $f(\infty) = 1$ .

Now, the proposed model is characterized by  $\alpha$ ,  $\beta$ ,  $N$ , and  $N_{\text{tot}}$  which act as the controlling parameters for the nonequilibrium steady-state properties. To reduce the number of parameters under consideration, we define a filling factor  $\mu$  as  $\mu = \frac{N_{\text{tot}}}{4N}$  which keeps track of the total number of particles [ $N_p(t)$  + count of particles on all the lanes] in the system with respect to the total number of sites in the system. Thus the controlling parameters for the system reduce to entrance-exit rates and the filling factor  $\mu$ .

### III. MASTER EQUATIONS AND MEAN-FIELD ANALYSIS

We characterize the occupancy status of each site for every lane by the symbols  $\tau_j^{+,i}$  and  $\tau_j^{-,i}$  for the positive and the negative species, respectively. Here,  $i \in \{1, 2, \dots, N\}$  indicates the

site number and  $j \in \{P, B_{\pm}, Q\}$  represents the corresponding lane. The governing densities of the bulk sites ( $1 < i < N$ ) for the bidirectional lanes ( $j = P, Q$ ) employing the master equations can be described as follows:

$$\begin{aligned} \frac{d\langle \tau_j^{+,i} \rangle}{dt} &= \langle \tau_j^{+,i-1} (1 - \tau_j^{+,i} - \tau_j^{-,i}) \rangle + \langle \tau_j^{+,i-1} \tau_j^{-,i} \rangle \\ &\quad - \langle \tau_j^{+,i} (1 - \tau_j^{+,i+1} - \tau_j^{-,i+1}) \rangle - \langle \tau_j^{+,i} \tau_j^{-,i+1} \rangle, \\ \frac{d\langle \tau_j^{-,i} \rangle}{dt} &= \langle \tau_j^{-,i+1} (1 - \tau_j^{-,i} - \tau_j^{+,i}) \rangle + \langle \tau_j^{-,i+1} \tau_j^{+,i} \rangle \\ &\quad - \langle \tau_j^{-,i} (1 - \tau_j^{-,i-1} - \tau_j^{+,i-1}) \rangle - \langle \tau_j^{-,i} \tau_j^{+,i-1} \rangle. \end{aligned} \quad (3)$$

Here, the notation  $\langle \dots \rangle$  denotes the statistical average. In the above equations, the positive and the negative terms on the right-hand sides correspond to the gain and loss of particles on the lane concerning the hopping and the swapping of the two species.

Similarly, for the bridge lanes, the particle evolution equations for the bulk can be written as

$$\begin{aligned} \frac{d\langle \tau_{B_+}^{+,i} \rangle}{dt} &= \langle \tau_{B_+}^{+,i-1} (1 - \tau_{B_+}^{+,i}) \rangle - \langle \tau_{B_+}^{+,i} (1 - \tau_{B_+}^{+,i+1}) \rangle, \\ \frac{d\langle \tau_{B_-}^{-,i} \rangle}{dt} &= \langle \tau_{B_-}^{-,i+1} (1 - \tau_{B_-}^{-,i}) \rangle - \langle \tau_{B_-}^{-,i} (1 - \tau_{B_-}^{-,i-1}) \rangle. \end{aligned}$$

After simplification, the particle evolution equations for all the lanes of the system can be written as

$$\begin{aligned} \frac{d\langle \tau_j^{+,i} \rangle}{dt} &= \langle \tau_j^{+,i-1} (1 - \tau_j^{+,i}) \rangle - \langle \tau_j^{+,i} (1 - \tau_j^{+,i+1}) \rangle, \\ \frac{d\langle \tau_j^{-,i} \rangle}{dt} &= \langle \tau_j^{-,i+1} (1 - \tau_j^{-,i}) \rangle - \langle \tau_j^{-,i} (1 - \tau_j^{-,i-1}) \rangle. \end{aligned} \quad (4)$$

Now, all the equations governing the evolution of particles in each lane are decoupled, however, these equations are intractable in their present form due to the involvement of two-point correlators. So, we employ mean-field approximation which has worked as a vital tool to explore the behavior of numerous many-body systems [16,17,22,34]. Mean-field in

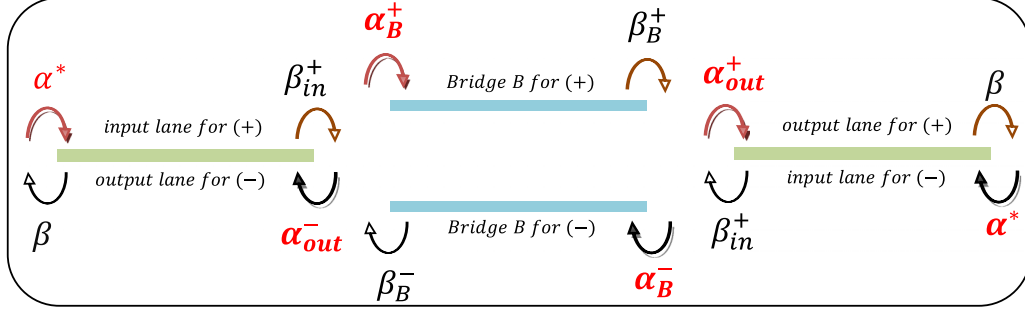


FIG. 2. Representation of the proposed model with the fictitious defined entrance and exit rates through each lane required for analytical treatment.

its simplest form neglects all the spatial correlations between neighboring particles and considers the occupancy of two adjacent sites to be independent of each other. To obtain the continuum limit of the model, we coarse grain the discrete lane with constant  $\epsilon = 1/N$  and re-scaled time as  $t' = t/N$ . In the continuum limit, the variables  $\langle \tau_j^{+,i} \rangle$  and  $\langle \tau_j^{-,i} \rangle$  are replaced with  $\rho_j^{+,i}$  and  $\rho_j^{-,i}$  and using the terms up to second order in the Taylor series expression, we obtain

$$\frac{\partial}{\partial t'} \left[ \rho_j^+ \right] = \frac{\partial}{\partial x} \left[ \frac{\epsilon}{2} \frac{\partial \rho_j^+}{\partial x} - \rho_j^+ (1 - \rho_j^+) \right], \quad (5)$$

$$\frac{\partial}{\partial t'} \left[ \rho_j^- \right] = \frac{\partial}{\partial x} \left[ \frac{\epsilon}{2} \frac{\partial \rho_j^-}{\partial x} + \rho_j^- (1 - \rho_j^-) \right].$$

The superscript  $i$  was dropped as the lanes are free from in-homogeneity of any type. At steady state, the above equation reduces to

$$\frac{\epsilon}{2} \frac{\partial^2 \rho_j^+}{\partial x^2} + (2\rho_j^+ - 1) \frac{\partial \rho_j^+}{\partial x} = 0, \quad (6)$$

$$\frac{\epsilon}{2} \frac{\partial^2 \rho_j^-}{\partial x^2} - (2\rho_j^- - 1) \frac{\partial \rho_j^-}{\partial x} = 0.$$

In the limit  $\epsilon \rightarrow 0$ , this equation yields  $\frac{\partial J_j^\pm}{\partial x} = 0$ , where  $J_j^\pm$  gives us the bulk current of each species of particle as

$$J_j^+ = \rho_j^+ (1 - \rho_j^+), \quad J_j^- = \rho_j^- (1 - \rho_j^-). \quad (7)$$

In the following section, we intend to utilize mean-field approximation to examine the stationary properties of the proposed model. To appropriately connect lanes P and Q with the bridge lanes, we must first define the effective entrance and exit rates for each lane. Further, we make use of notations  $\rho_j^{+,i}$  and  $\rho_j^{-,i}$  to represent the average particle density of the (+) and (-) particle, respectively, on site  $i$  in the  $j$ th lane. Moreover, the average densities in the bulk will be denoted by  $\rho_j^+$  and  $\rho_j^-$ . The current induced by the (+) and (-) particles in each lane will be denoted by  $J_j^+$  and  $J_j^-$ . Also, the symbol  $J_j^{k,1}$  and  $J_j^{k,N}$  is used to describe the current at the boundary sites on each lane. Considering that lane P (Q) operates as an input(output) lane for the positive (negative) species and lane Q (P) as an output (input) lane for positive (negative) particles, for analytical amenability we prefer to take that  $j \in \{\text{in}, B, \text{out}\}$  for the rest of the article, where  $B$  stands for the respective bridge lane.

### A. Dynamics of lanes P and Q

For the thorough theoretical investigation, we need to define effective entrance and exit rates for lanes P and Q. Taking into account that lane P (Q) acts as an input lane for positive (negative) particles and lane Q (P) behaves as an output lane for the negative (positive) species, we define the effective exit rate of (+) and (-) particles from the lane P and Q through the site  $i = N$  and  $i = 1$ , as  $\beta_{\text{in}}^+$  and  $\beta_{\text{in}}^-$ , respectively (see Fig. 2). Similarly, the effective entrance rate of (+)/(-) particles from bridge lane  $B_+/B_-$  to lane Q/P is denoted by  $\alpha_{\text{out}}^+/\alpha_{\text{out}}^-$ .

Following mean-field approximation and the current continuity condition, the current flowing out of lane P (Q) is equal to the current passing from lane P(Q) to the bridge lane  $B_+(B_-)$ , which gives

$$\beta_{\text{in}}^+ \rho_{\text{in}}^{+,N} = \rho_{\text{in}}^{+,N} (1 - \rho_B^{+,1}), \quad (8)$$

$$\beta_{\text{in}}^- \rho_{\text{in}}^{-,1} = \rho_{\text{in}}^{-,1} (1 - \rho_B^{-,N}),$$

and can be simplified to obtain

$$\beta_{\text{in}}^+ = 1 - \rho_B^{+,1}, \quad (9)$$

$$\beta_{\text{in}}^- = 1 - \rho_B^{-,N}.$$

Similarly, the current continuity argument suggests that the current passing through the bridge lane to lane Q/P must be equal to the inflow of current in lane Q/P, which can be written as

$$\alpha_{\text{out}}^+ (1 - \rho_{\text{out}}^{+,1} - \rho_{\text{in}}^{-,1}) = \rho_B^{+,N} (1 - \rho_{\text{out}}^{+,1} - \rho_{\text{in}}^{-,1}), \quad (10)$$

$$\alpha_{\text{out}}^- (1 - \rho_{\text{in}}^{+,N} - \rho_{\text{out}}^{-,N}) = \rho_B^{-,1} (1 - \rho_{\text{in}}^{+,N} - \rho_{\text{out}}^{-,N}),$$

which implies

$$\alpha_{\text{out}}^+ = \rho_B^{+,N}, \quad (11)$$

$$\alpha_{\text{out}}^- = \rho_B^{-,1}.$$

Next, we utilize the continuity of current within the bulk and at the boundaries of each lane to further analyze lane P. Subsequently, we extend a similar treatment to lane Q. According to the mean-field approximation, the bulk current of each species of particle on lane P can be expressed as

$$J_{\text{in}}^+ = \rho_{\text{in}}^+ (1 - \rho_{\text{in}}^+), \quad J_{\text{out}}^- = \rho_{\text{out}}^- (1 - \rho_{\text{out}}^-). \quad (12)$$

Similarly, the boundary currents are given by

$$\begin{aligned} J_{\text{in}}^{+,1} &= \alpha^* (1 - \rho_{\text{in}}^{+,1} - \rho_{\text{out}}^{-,1}), & J_{\text{in}}^{+,N} &= \beta_{\text{in}}^+ \rho_{\text{in}}^{+,N}, \\ J_{\text{out}}^{-,N} &= \alpha_{\text{out}}^- (1 - \rho_{\text{in}}^{+,N} - \rho_{\text{out}}^{-,N}), & J_{\text{out}}^{-,1} &= \beta_{\text{out}}^- \rho_{\text{out}}^{-,1}. \end{aligned} \quad (13)$$

Since, in the stationary state, the current is continuous throughout the lane, one can simply write that

$$\begin{aligned} J_{\text{in}}^{+,1} &= J_{\text{in}}^{+,2} = \dots = J_{\text{in}}^{+,N} = J_{\text{in}}^+, \\ J_{\text{out}}^{-,1} &= J_{\text{out}}^{-,2} = \dots = J_{\text{out}}^{-,N} = J_{\text{out}}^-. \end{aligned} \quad (14)$$

It can be easily observed from Eqs. (12) and (13), the two bulk currents for the different species are decoupled and they interact effectively only at the boundaries. Therefore, lane P can be viewed as two independent single-species TASEP lanes with are connected through the boundaries only. Under this consideration, it is reasonable to define the modified entrance rates [16,22] for the two species to lane P by utilizing the current continuity condition described in Eq. (14), as

$$\alpha_{\text{in,eff}}^+ = \frac{J_{\text{in}}^+}{\frac{J_{\text{in}}^+}{\alpha^*} + \frac{J_{\text{out}}^-}{\beta}}, \quad \alpha_{\text{out,eff}}^- = \frac{J_{\text{out}}^-}{\frac{J_{\text{out}}^-}{\alpha_{\text{out}}^-} + \frac{J_{\text{in}}^+}{\beta_{\text{in}}^+}}. \quad (15)$$

As lane Q also portrays bidirectional flow, an analogous argument can be utilized to define the modified entrance rates for the different particle species which results in

$$\alpha_{\text{out,eff}}^+ = \frac{J_{\text{out}}^+}{\frac{J_{\text{out}}^+}{\alpha_{\text{out}}^+} + \frac{J_{\text{in}}^-}{\beta_{\text{in}}^-}}, \quad \alpha_{\text{in,eff}}^- = \frac{J_{\text{in}}^-}{\frac{J_{\text{in}}^-}{\alpha^*} + \frac{J_{\text{out}}^+}{\beta}}. \quad (16)$$

### B. Dynamics of bridge lanes

We define that a positive particle can enter bridge lane  $B_+$  from the lane P with an effective entrance rate  $\alpha_B^+$  and can leave this lane with an effective exit rate  $\beta_B^+$  as depicted in Fig. 2. Similarly, a negative particle from lane Q can enter the bridge  $B_-$  with rate  $\alpha_B^-$  and can exit to lane P with an effective exit rate of  $\beta_B^-$ .

The flow of each species of particle must remain continuous, which suggests that the current passing from the lane P/Q to  $B_+/B_-$  lane must be equal to the current entering the bridge lane, and can be written as

$$\begin{aligned} \alpha_B^+ (1 - \rho_B^{+,1}) &= \rho_{\text{in}}^{+,N} (1 - \rho_B^{+,1}), \\ \alpha_B^- (1 - \rho_B^{-,N}) &= \rho_{\text{out}}^{-,1} (1 - \rho_B^{-,N}). \end{aligned} \quad (17)$$

Similarly, the exit current from the bridge lane can be equated to the currents passing from the bridge lane to lane Q/P as

$$\begin{aligned} \beta_B^+ \rho_B^{+,N} &= \rho_B^{+,N} (1 - \rho_{\text{out}}^{+,1} - \rho_{\text{in}}^{-,1}), \\ \beta_B^- \rho_B^{-,1} &= \rho_B^{-,1} (1 - \rho_{\text{in}}^{+,N} - \rho_{\text{out}}^{-,N}). \end{aligned} \quad (18)$$

The above two equations can be simplified to obtain

$$\begin{aligned} \alpha_B^+ &= \rho_{\text{in}}^{+,N}, & \alpha_B^- &= \rho_{\text{out}}^{-,1}, \\ \beta_B^+ &= 1 - \rho_{\text{out}}^{+,1} - \rho_{\text{in}}^{-,1}, & \beta_B^- &= 1 - \rho_{\text{in}}^{+,N} - \rho_{\text{out}}^{-,N}. \end{aligned} \quad (19)$$

### C. Boundary dynamics

The first site ( $i = 1$ ) of lane P and the last site ( $i = N$ ) of lane Q is connected to a pool having a finite number of particles. As the total number of particles in the system remains

conserved, one can write

$$N_{\text{tot}} = N_p + N_P + N_Q + N_{B_+} + N_{B_-}, \quad (20)$$

where  $N_j$ ,  $j \in \{P, Q, B_+, B_-\}$  signifies the count of the number of positive and negative species on lane  $j$ . At steady state, we can write these quantities as

$$\begin{aligned} N_P &= N \left( \int_0^1 \rho_{\text{in}}^+ dx + \int_0^1 \rho_{\text{out}}^- dx \right), \\ N_{B_+} &= N \int_0^1 \rho_B^+ dx, \\ N_{B_-} &= N \int_0^1 \rho_B^- dx, \\ N_Q &= N \left( \int_0^1 \rho_{\text{out}}^+ dx + \int_0^1 \rho_{\text{in}}^- dx \right). \end{aligned} \quad (21)$$

Thus, Eq. (20) becomes

$$N_{\text{tot}} = N_p + N \left( \int_0^1 \sum_{j \in \{\text{in}, B, \text{out}\}} (\rho_j^+ + \rho_j^-) dx \right). \quad (22)$$

To reduce the number of parameters to be investigated, the above equation can be rewritten as

$$\mu = r + \frac{1}{4} \left( \int_0^1 \sum_{j \in \{\text{in}, B, \text{out}\}} (\rho_j^+ + \rho_j^-) dx \right), \quad (23)$$

where  $r = \frac{N_p}{4N}$  defines the pool quotient. Thus, the effective entrance rate is given by Eq. (1) is modified to  $\alpha^* = \alpha \frac{r}{\mu}$ .

## IV. ANALYTIC PREDICTIONS

The steady-state dynamics and properties of the most basic version of the TASEP model on a single lane, where a particle enters a lane with the rate  $\alpha$ , moves along the bulk with unit rate and leaves with rate  $\beta$ , are exactly known [5]. In this case, the rates  $\alpha$  and  $\beta$  act as the boundary-controlling parameters resulting in three stationary phases: low-density phase (LD), high-density phase (HD), and maximal current phase (MC). However, a new type of phase called the shock (S) phase appears in the system when a constraint on the total number of particles is considered [51]. In the S phase, the particle density changes from LD to the HD phase and is localized. The shock is localized to a small region in the  $\alpha - \beta$  phase plane, depending upon the total number of particles. For the sake of completeness, we have summarized the observed outcomes such as the particle densities on each site, particle current along the existential region of each phase as well as the value of the effective entrance rate  $\alpha^*$  for each phase, in Table I. In the table, the bulk density is denoted by  $\rho^{\text{bulk}}$  while the left and right boundary density is signified as  $\rho^1$  and  $\rho^N$ , respectively.  $J$  is the position-independent steady-state particle current.

In a one-dimensional system with constrained resources, the steady-state particle densities are governed by the three controlling parameters ( $\alpha, \beta, \mu$ ). So, it is natural to assume that, it is also true in our situation except that now, the density profiles depend upon the effective entrance and exit rates of each lane, which have to be calculated in a self-consistent

TABLE I. Summary of the results for a one-dimensional lane with finite resources having entrance rate  $\alpha^*$ , exit rate  $\beta$ , and filling factor  $\mu = N_{\text{tot}}/N$ . Here, LD signifies the low-density phase, HD denotes the high-density phase, MC refers to Maximal current and the variable  $x_w$  indicates the position of shock in the shock (S) phase.

| Phase | $\rho^1$                              | $\rho^{\text{bulk}}$  | $\rho^N$                             | Current ( $J$ )                                  | Phase region                        | $\alpha^*$                         |
|-------|---------------------------------------|---|--------------------------------------|--|-------------------------------------|------------------------------------|
| LD    | $\alpha^*$                            | $\alpha^*$  | $\frac{\alpha^*(1-\alpha^*)}{\beta}$ | $\alpha^*(1-\alpha^*)$                           | $\alpha^* < \min\{0.5, \beta\}$     | $\alpha(\frac{\mu^2}{\mu+\alpha})$ |
| HD    | $1 - \frac{\beta(1-\beta)}{\alpha^*}$ | $1 - \beta$   | $1 - \beta$                          | $\beta(1 - \beta)$                               | $\beta < \min\{0.5, \alpha\}$       | $\alpha(1 - \frac{1-\beta}{2\mu})$ |
| MC    | $1 - \frac{1}{4\alpha^*}$             | 0.5   | $\frac{1}{4\beta}$                   | 0.25   | $0.5 < \min\{\alpha^*, \beta\}$     | $\alpha(1 - \frac{\mu}{2\mu})$     |
| S     | $\alpha^*$                            | $\begin{cases} \alpha^* & \text{if } 0 < x_w \\ 1 - \beta & \text{if } x_w < 1 \end{cases}$ | $1 - \beta$                          | $\alpha^*(1 - \alpha^*)$<br>$= \beta(1 - \beta)$ | $\alpha^* = \beta$<br>$0 < x_w < 1$ | $\beta$                            |

manner. By plugging the appropriate values of the densities at the boundary sites, the values of effective and modified rates can be calculated from Eqs. (1), (9), (11), (15), (16), (19), and (23).

To begin, we first define the notion of labeling a possible phase in a phase diagram. Any given density profile can be expressed as  $X_1 - X_2 - X_3/Y_1 - Y_2 - Y_3$ . In this notation,  $X_1, X_2$ , and  $X_3$  represent the phases exhibited by the positive particles in lane P, bridge  $B_+$ , and lane Q, respectively. Similarly,  $Y_1, Y_2$ , and  $Y_3$  denote the phases displayed by the negative particles in lane Q, bridge  $B_-$ , and lane P, respectively. Additionally, by observing the phase exhibited by individual particle species in each lane, we identify whether the overall system's phase is symmetric or asymmetric. In the case of a symmetric phase, the bulk densities of both the particle species in their respective lanes are equal, i.e.,  $\rho_{\text{in}}^+ = \rho_{\text{in}}^-$ ,  $\rho_B^+ = \rho_B^-$ ,  $\rho_{\text{out}}^+ = \rho_{\text{out}}^-$ ; meanwhile for asymmetric phases, the characteristics including currents and density profiles are generally different for the two-particle species.

The two-particle species can exhibit four possible phases in each lane, leading to a total of  $4^6 = 4096$  phases displayed by the system. Clearly, listing all probable phases is not admissible. Since a phase of the form,  $X_1 - X_2 - X_3/Y_1 - Y_2 - Y_3$  is equivalent to  $Y_1 - Y_2 - Y_3/X_1 - X_2 - X_3$ , that is the changing the role of the two species has no impact on the phase displayed, the number of phases gets reduced to 2080. The majority of these cases, however, cannot exist because of several constraints and are discussed in Appendix C. Now, based on the observed stationary properties, including density profiles, effective entrance rates, and particle currents, we categorize the different phases as either symmetric or asymmetric.

### A. Symmetric phases

During a symmetric phase, the system displays identical stationary properties for both the particle species, including particle densities and currents in each lane. This equivalence arises due to the consistency of the dynamical processes and the behavior of the system which is indistinguishable between the two particle types. Such a circumstance gives

$$\begin{aligned} J_{\text{in}}^+ &= J_{\text{in}}^-, & J_{\text{in}}^- &= J_{\text{out}}^+, & J_B^+ &= J_B^-, \\ \rho_{\text{in}}^+ &= \rho_{\text{out}}^-, & \rho_{\text{in}}^- &= \rho_{\text{out}}^+, & \rho_B^+ &= \rho_B^-, \end{aligned} \quad (24)$$

leading to

$$\begin{aligned} \beta_{\text{in}}^+ &= \beta_{\text{in}}^- = \beta_{\text{in}}, \\ \alpha_B^+ &= \alpha_B^- = \alpha_B, \\ \beta_B^+ &= \beta_B^- = \beta_B, \\ \alpha_{\text{out}}^+ &= \alpha_{\text{out}}^- = \alpha_{\text{out}}. \end{aligned} \quad (25)$$

This implies that modified entrance rates described by the Eqs. (15) and (16) alters to

$$\begin{aligned} \alpha_{\text{in,eff}}^+ &= \alpha_{\text{in,eff}}^- = \frac{J_{\text{in}}}{\frac{J_{\text{in}}}{\alpha^*} + \frac{J_{\text{out}}}{\beta}} = \alpha_{\text{in,eff}}, \\ \alpha_{\text{out,eff}}^+ &= \alpha_{\text{out,eff}}^- = \frac{J_{\text{out}}}{\frac{J_{\text{out}}}{\alpha_{\text{out}}} + \frac{J_{\text{in}}}{\beta_{\text{in}}}} = \alpha_{\text{out,eff}}, \end{aligned} \quad (26)$$

where  $J_{\text{in}}^+ = J_{\text{in}}^- = J_{\text{in}}$  and  $J_{\text{out}}^+ = J_{\text{out}}^- = J_{\text{out}}$ . Therefore, utilizing the above conditions, one can calculate the effective entrance and exit rates of all the lanes and finally obtain the stationary density profile of a symmetric phase. We've used abbreviations (LD, HD, MC, SP) to indicate lane phases in a symmetrical context- LD representing low-density, HD for high-density, MC for maximal current phase, and SP for the shock phase.

As a result, there are  $4^3 = 64$  possible symmetric phases out of which there are only four achievable phases: LD-LD-LD/LD-LD-LD, LD-SP-LD/LD-SP-LD, SP-HD-LD/SP-HD-LD, and HD-HD-LD/HD-HD-LD. The rest of the phases are discarded based upon either physical or mathematical argument for which the complete explanations is detailed in Appendix C. For the feasible phase, we provide the explicit expressions for the particle densities, currents, position of the shock, and the phase boundaries in Appendix A.

### B. Asymmetric phases

In our model, the two species of particles interact effectively at the boundaries of lane P as well as lane Q which is the sole factor affecting the symmetry between the distinct particle species. This leads to the emergence of the asymmetrical phases and subsequently, spontaneous symmetry breaking phenomena. In an asymmetric phase, each species exhibits distinctive properties in terms of current and density, and this section examines the likelihood of the occurrence of such phases. To simplify the analysis, it is assumed that the positive particles outnumber the negative ones. To distinguish an

asymmetrical phase from a symmetrical phase, we have used the notation of L for low-density, H for high-density, M for the maximal current phase, and S for the shock phase.

Theoretical investigation of such phases reveals that there are 11 attainable asymmetric phases for which the existence criteria, expressions of shock position, and effective entrance rates wherever possible are explained in Appendix B. The remaining phases are eliminated based on theoretical reasoning, which is presented in Appendix C.

## V. RESULTS: ANALYSIS AND IMPLICATIONS

To explore the dynamics of the system in the steady state, we create phase diagrams in the parameter space  $(\alpha, \beta)$  based on our theoretical investigations explained in the previous section as well as Appendices A and B. The objective is to examine how the system's complex dynamics are affected by the global constraint on the resources available which is quantified by the variable  $\mu$ . To verify our theoretical findings, we conduct Monte Carlo simulations (MCs) utilizing the Gillespie Algorithm which is detailed in Appendix E. It has been observed that the consistency between simulation data and analytical predictions holds true across all regimes. Alternatively, we can employ numerical techniques (refer to Appendix D) on the continuum version of the particle evolution equation, represented by Eq. (5), to obtain density profiles for any given phase. There are several advantages of adopting this approach. First, it is easier to implement compared to the analytical methods outlined in Appendices A and B. Second, unlike the theoretical approach, this method can be readily adapted to more generalized models by incorporating changes in the master equation. Last, this approach allows for obtaining solutions in cases where the choice of functions in Eq. (2) leads to analytically intractable forms.

### A. Role of filling factor

Using the analytical findings presented in Secs. IV A and IV B, we proceed to explicitly establish the mathematical expressions for the phase boundaries, whenever feasible, that distinguish the two phases. These phase boundaries are vital in discerning various phase configurations.

(1) The boundary separating the LD-LD-LD/LD-LD-LD phase from LD-SP-LD/LD-SP-LD as obtained from Eq. (A2) is

$$\beta = \frac{\alpha(2\mu - 1)}{3\alpha(\mu - 1) - 2\mu}. \quad (27)$$

(2) For the LD-SP-LD/LD-SP-LD phase to LD-HD-LD/LD-HD-LD, the boundary is expressed as

$$\beta = \frac{\alpha(3\mu - 2)}{3\alpha(3\mu - 2) - \mu}, \quad (28)$$

which is calculated from Eq. (A3) by solving  $x_w = 0$ .

(3) For the symmetric LD-LD-LD/LD-LD-LD to L-L-L/L-L-L, we have

$$\alpha_{\text{out,eff}}^- = \beta,$$

where  $\alpha_{\text{out,eff}}^-$  is given by Eq. (B1).

(4) The boundary between the L-L-S/L-L-L and L-S-H/L-L-L phases can be identified from Eq. (B4) by setting  $x_w = 0$  which can be realized as L-L-H/L-L-L phase.

(5) Boundary separating the L-S-H/L-L-L and S-H-H/L-L-L phases, as determined by Eq. (B6) with  $x_w = 0$ , corresponds to the L-H-H/L-L-L phase.

(6) For the S-H-H/L-L-L and H-H-H/L-L-L phase the boundary is represented as

$$\alpha_{\text{in,eff}}^+ = \beta, \quad (29)$$

for  $\alpha_{\text{in,eff}}^+$  given in Eq. (B2).

To perform a comprehensive analysis, we present phase diagrams for specific values of  $\mu$  spanning from 0 to  $\infty$ . These diagrams exhibit significant topological changes in the parameter space  $(\alpha, \beta)$  and are visually represented in Fig. 3. The figures are generated using carefully selected values of  $\mu$  to highlight noteworthy modifications in the structure of the phase diagrams.

When the system contains only a small number of particles, approximately  $\mu \approx 0.001$ , a single symmetric phase, namely LD-LD-LD/LD-LD-LD, is observed. The scarcity of particles limits the effective particle influx into the lane, resulting in the manifestation of a low-density phase in each lane. With the addition of more particles to the system, the number of phases increases to three. The phase diagram then consists of one symmetric phase (LD-LD-LD/LD-LD-LD) and two asymmetric phases (L-L-L/L-L-L and L-L-S/L-L-L), which disrupt the symmetry of the system as evident from Fig. 3(a) for  $\mu = 0.1$ . This observation can be explained as follows: For lower values of  $\beta$ , there is a tendency for particles to accumulate primarily at the right end of the output lane. Consequently, the boundary layer at the right boundary infiltrates into the bulk region, resulting in the occurrence of a boundary-induced shock in the output lane.

Further increasing the particle count in the system reveals the emergence of two additional asymmetric phases: L-L-H/L-L-L and L-S-H/L-L-L, as depicted in Fig. 3(b) for  $\mu = 0.45$ . The L-S-H/L-L-L phase appears adjacent to L-L-S/L-L-L, with L-L-H/L-L-L serving as a boundary curve that separates the L-L-S/L-L-L and L-S-H/L-L-L phase regions. When the value of  $\mu$  exceeds 0.5, two new asymmetric phases, namely L-H-H/L-L-L and S-H-H/L-L-L, emerge alongside the L-S-H/L-L-L phase. Additionally, a symmetric phase (LD-SP-LD/LD-SP-LD) appears adjacent to the LD-LD-LD/LD-LD-LD phase, in addition to the already existing phases. Physically, the emergence of the high-density (HD) phase in a lane is expected, as it cannot occur in the system for  $\mu < 0.5$  due to an insufficient number of particles in the system to achieve the high-density state. The critical value of  $\mu$  at which the bulk-induced shock phase (LD-SP-LD/LD-SP-LD) emerges is 0.5 and is theoretically justified from Eq. (27). Furthermore, the L-H-H/L-L-L phase acts as a boundary curve that separates the S-H-H/L-L-L and L-S-H/L-L-L phase regions [see phase diagram given Fig. 3(c) for  $\mu = 0.6$ ].

Beyond  $\mu = 0.5$ , the topology of the phase diagram undergoes substantial qualitative and quantitative changes. The phase plane becomes more intricate due to the emergence of new symmetrical and asymmetrical phases as evident

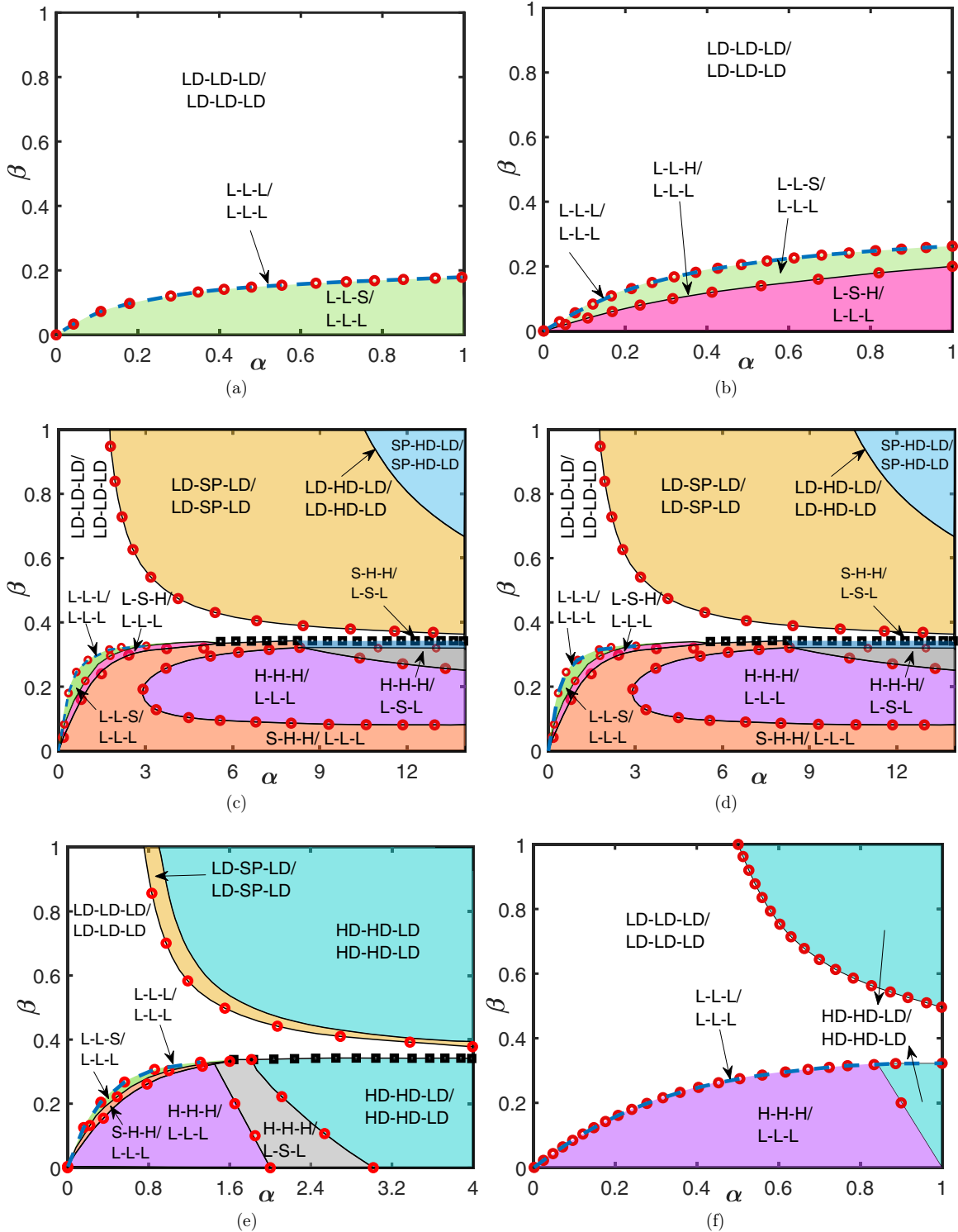


FIG. 3. Stationary phase diagrams for different values of  $\mu$ : (a)  $\mu = 0.1$ , (b)  $\mu = 0.45$ , (c)  $\mu = 0.6$ , (d)  $\mu = 0.7$ , (e)  $\mu = 1.5$ , and (f)  $\mu \rightarrow \infty$ . Solid lines represent theoretical findings while red circles denote Monte Carlo simulation results. The blue dashed curves indicates the L-L-L/L-L-L phase. The phases L-L-L/L-L-L, L-L-S/L-L-L, L-L-H/L-L-L, L-S-H/L-L-L, and L-H-H/L-L-L, all converge in a narrow region which is presented by black squares in panels (d) and (e).

from Fig. 3(d) for  $\mu = 0.7$ . Consequently, the phase diagram undergoes changes such as the translation of phase boundaries and contraction of existing phases. Notably, four new asymmetrical phases, specifically H-H-H/L-L-L, H-H-H/L-S-L, S-H-H/L-S-L, and L-H-H/L-S-L appear in the

phase plane. Additionally, two symmetrical phases, LD-HD-LD/LD-HD-LD and SP-HD-LD/SP-HD-LD, emerge. The symmetric phase SP-HD-LD/SP-HD-LD appears adjacent to the symmetric LD-SP-LD/LD-SP-LD phase, and the boundary separating these two phases represents the

LD-HD-LD/LD-HD-LD phase. The Eq. (28) provides the curve indicating the existence of the LD-HD-LD/LD-HD-LD phase. In the lower half region, when  $\alpha$  takes on large values, a significant portion of the region is dominated by the H-H-H/L-L-L phase, which is adjacent to the S-H-H/L-L-L phase. Figure 3(d) illustrates that for  $\alpha \approx 5.5$ , the boundary curves corresponding to L-L-L/L-L-L, L-L-H/L-L-L, and L-H-H/L-L-L all converge within a very narrow region of width approximately 0.02 with respect to  $\beta$ . Consequently, this narrow region is represented by 'black square' symbols in the phase diagram. The coordinates  $(\bar{\alpha}, \bar{\beta})$  in the  $\alpha$ - $\beta$  plane, where the two curves represent the boundary of the H-H-H/L-L-L region given by Eq. (B3) intersect, can be easily determined. This intersection occurs at the points where  $\alpha_{\text{in,eff}}^- + \alpha_{\text{out,eff}}^- = \alpha_{\text{in,eff}}^+$ . For a fixed value of  $\alpha \geq \bar{\alpha}$ , an increase in the value of  $\beta$  leads to a phase transition sequence: H-H-H/L-L-L  $\rightarrow$  H-H-H/L-S-L  $\rightarrow$  S-H-H/L-S-L  $\rightarrow$  L-H-H/L-S-L  $\rightarrow$  L-S-H/L-L-L  $\rightarrow$  L-L-H/L-L-L  $\rightarrow$  L-L-S/L-L-L  $\rightarrow$  L-L-L/L-L-L  $\rightarrow$  LD-LD-LD/LD-LD-LD.

Once  $\mu$  exceeds the value 1, a new symmetric phase emerges in the phase diagram, referred to as HD-HD-LD/HD-HD-LD [see Fig. 3(e)]. In this phase, the HD (high-density) region always maintains a maximal particle density of 1, while the low-density region remains at 0. This phase can be interpreted as a congestion region, where there is no particle movement whatsoever. It is positioned adjacent to SP-HD-LD/SP-HD-LD in the upper half plane and is also neighboring the H-H-H/L-S-L phase in the lower half plane. Finally, as  $\mu \rightarrow \infty$ , the phase diagram undergoes a substantial simplification. It displays only four distinct stationary phases: two symmetric phases, namely LD-LD-LD/LD-LD-LD and HD-HD-LD/HD-HD-LD, and two asymmetric phases, L-L-L/L-L-L and H-H-H/L-L-L as evident from Fig. 3(f).

The aforementioned observations demonstrate that the presence of limited resources has a substantial impact on the phenomenon of symmetry breaking. This effect occurs even with a relatively small number of particles in the system. In the forthcoming sections, we will elucidate the significant and abrupt phase transitions discussed earlier, as well as delve into the dynamics of shocks both boundary-induced and bulk-induced.

### B. Shock dynamics

In this section, we will explore the characteristics of two distinct types of shocks that have been observed in the previous section. A shock that enters through either the left end of the input lane or the right end of an output lane is referred to as a boundary-induced shock. A bulk-induced shock refers to the occurrence of localized congestion within the interior of the system, away from the boundaries. It originates from the internal dynamics of the system rather than external influences at the boundaries. To delve into a detailed study of the phase transitions that lead to the formation of these types of shocks, we have selected a filling factor value and vary the boundary-controlling parameters  $\alpha$  and  $\beta$ .

A bulk-induced shock in the symmetric LD-SP-LD/LD-SP-LD and SP-HD-LD/SP-HD-LD appears in the phase diagram, as evident from Fig. 3(d). In the LD-SP-LD/LD-SP-LD, a discontinuity in the density profile is observed in the

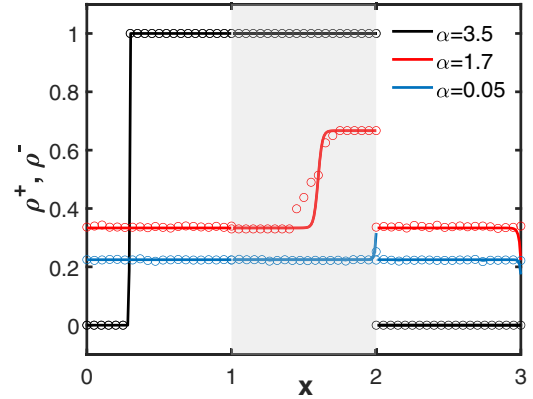


FIG. 4. Phase transitions exhibited for  $\mu = 0.8$  and  $\beta = 1$  for varying values of  $\alpha$ . The system evolves from LD-LD-LD/LD-LD-LD  $\rightarrow$  LD-SP-LD/LD-SP-LD  $\rightarrow$  SP-HD-LD/SP-HD-LD. Since in the symmetric phase, the density profiles for the two species are identical, we plot the density profile only for the positive species. Solid lines give mean-field results while symbols correspond to Monte Carlo simulations. The shaded region for  $x \in [1, 2]$  represents the bridge lane.

bridge lane for both particle species. While for the SP-HD-LD/SP-HD-LD, this discontinuity appears in the input lane, where the density profile connects a region of low density having constant particle density at 0 to a region of high density with density 1. The explicit expression for the location of the shock in LD-SP-LD/LD-SP-LD is computed in Eq. (A3) which suggest that for fixed values of  $\beta$  and  $\mu$ , an increase in  $\alpha$  leads to an increase in the number of particles feed into the system which in turn sweeps the shock toward the left. This is affirmed by Fig. 4, which clearly shows that for  $\beta = 1$  and  $\mu = 0.8$ , the high-density region of the shock enhances and with an increase in  $\alpha$ , the shock vanishes from the bridge lane. To validate it mathematically, we employ Eq. (A3), which gives us the shock position in the LD-SP-LD/LD-SP-LD phase as

$$x_w = \frac{6\beta\mu}{\alpha(3\beta - 1)} - 2(3\mu - 2).$$

The shock position clearly demonstrates that an increase in  $\alpha$  causes the shock to shift toward the left, indicating the disappearance of the LD-SP-LD/LD-SP-LD phase. With further enhancement in  $\alpha$ , this shock enters the input lane leading to an occurrence of the SP-HD-LD/SP-HD-LD phase. As already been examined theoretically, in this phase, a density profile connecting a region of density 0 to 1 is observed in the input lane, density 1 in the bridge lane, and the output lane has a constant density of 0 (see Appendix A).

Now, let us examine some key aspects of the localized shock induced by the boundary in the phase diagram for  $\mu = 0.6$ , as shown in Fig. 3(c). When a particular lane undergoes a shock phase, we can determine the speed of the shock by calculating the difference between the exit rate and the entrance rate of that specific lane. For the system to exhibit a localized shock, the speed of the shock must be zero. To analyze the behavior of the shock, we fix  $\mu = 0.6$  and  $\alpha = 2$ , and examine the position of the shock relative to the exit rate

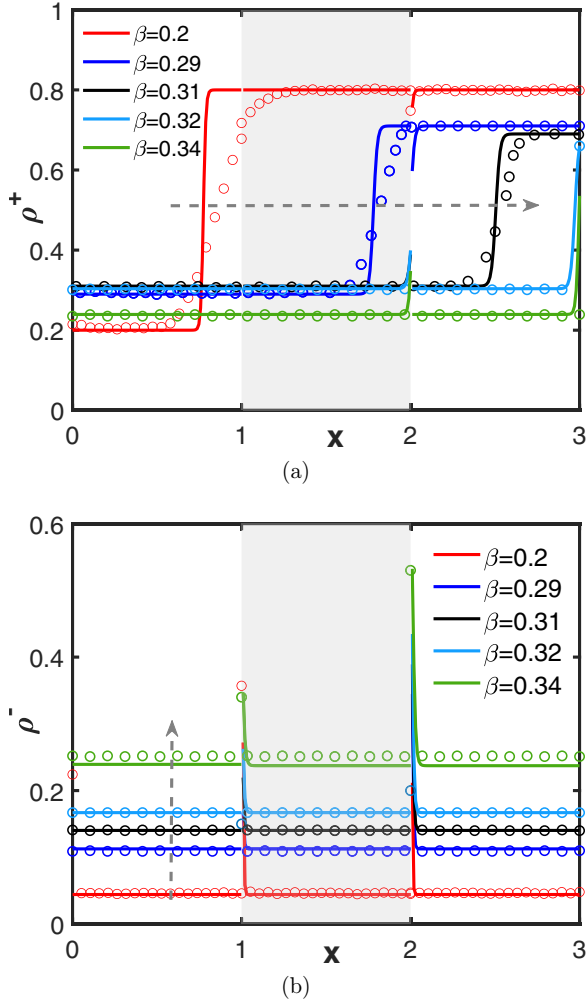


FIG. 5. Phase transitions with respect to  $\beta$  for fixed values of the other parameters as  $\alpha = 2$ , and  $\mu = 0.6$  representing evolution of the system from S-H-H/L-L-L  $\rightarrow$  L-S-H/L-L-L  $\rightarrow$  L-L-S/L-L-L  $\rightarrow$  L-L-L/L-L-L  $\rightarrow$  LD-LD-LD/LD-LD-LD. Panels (a) and (b) show the density profile for the (+) and the (-) species, respectively. Solid lines give mean-field results while symbols correspond to Monte Carlo simulations. The shaded region for  $x \in [1, 2]$  represents the bridge lanes. The dotted arrow indicates the direction of increasing  $\beta$ .

parameter  $\beta$ . Figure 5(a) illustrates the phase transitions of the positive species as  $\beta$  increases. We can observe the following sequence of transitions for the positive species: S-H-H  $\rightarrow$  L-H-H  $\rightarrow$  L-S-H  $\rightarrow$  L-L-H  $\rightarrow$  L-L-S  $\rightarrow$  L-L-L. Throughout these transitions, the negative species consistently exhibit a low-density phase in each lane. These transitions can be explained through the following reasoning. For smaller values of  $\beta$ , a shock enters the input lane of the positive particles from the left end. The position of this shock can be determined using Eq. (B6). As  $\beta$  increases, the effective entrance rate  $\alpha_{\text{in,eff}}^+$  also increases, causing the shock to move toward the right. With further increments in  $\beta$ , the shock travels from lane P to the bridge lane and then to lane Q, ultimately leaving the system and resulting in the positive particles displaying a low-density phase in each lane. Meanwhile the entrance rate of the negative species through lane Q which is  $\alpha_{\text{in,eff}}^-$  also continues to increase with respect to  $\beta$  [see Fig. 5(b)]. Thus,

if one considers the position of shock as the order parameter, then these transitions are of second order.

Here, we will explore the changes occurring in the  $\alpha$ - $\beta$  plane for  $\mu = 0.7$  by selecting a point within the H-H-H/L-L-L region, ensuring that  $\alpha$  is large enough. Our focus will be on examining the density profile at various values of  $\beta$  (refer to Fig. 6). To begin, we set  $\beta = 0.25$  in this region and present Fig. 6(a), where we observe an enhancement in the modified entrance rates of the two-particle species, given by  $\alpha_{\text{in,eff}}^\pm$ , as  $\beta$  increases. Initially, a bulk-induced shock phase, referred to as H-H-H/L-S-L, emerges in the system, characterized by a discontinuous density profile in the bridge lane for the negative species. As  $\beta$  further increases, a shock enters from the left end corresponding to the positive particles. This leads to a transition from the H-H-H/L-L-L phase to a bulk-induced shock phase H-H-H/L-S-L and finally to a boundary-induced shock phase S-H-H/L-S-L. Importantly, as  $\beta$  increases, both shocks progressively shift from the left to the right. Around the critical value of  $\beta \approx 0.332$ , the shock in lane P reaches the right boundary, causing the shock in the bridge lane to reverse its direction. As  $\beta$  further increases, the latter shock moves back toward the left boundary, resulting in the system transitioning into the L-H-H/L-L-L phase. After attaining this phase the system evolves to L-S-H/L-L-L  $\rightarrow$  L-L-H/L-L-L  $\rightarrow$  L-L-S/L-L-L  $\rightarrow$  L-L-L/L-L-L, whose details have already been discussed.

### C. Back-and-forth transitions

We now examine a special characteristic in the phase diagram known as the back-and-forth transition, which emerges when observing the phase diagram for  $\mu = 0.7$  [see Fig. 3(d)] and in the limit as  $\mu$  approaches infinity [see Fig. 3(f)]. The term ‘‘back-and-forth transition’’ is defined as follows. When examining a particular phase diagram, if the system undergoes a transition from phase X to phase Y and then returns back to phase X, denoted as X  $\rightarrow$  Y  $\rightarrow$  X while adjusting a single parameter and keeping the remaining parameters constant, we refer to this phenomenon as the back-and-forth transition [29,53,54].

Upon closer examination of the phase diagram for  $\mu = 0.7$ , an interesting boundary emerges between the S-H-H/L-L-L and H-H-H/L-L-L regions. When we analyze the system’s behavior by fixing  $\alpha = 4$ ,  $\mu = 0.7$  and only varying the exit rate  $\beta$ , we observe a transition from the S-H-H/L-L-L phase to the H-H-H/L-L-L phase. Surprisingly, as  $\beta$  continues to increase, the system transitions back to the S-H-H/L-L-L phase. Equation (29) provides us with the phase boundary between the S-H-H/L-L-L and H-H-H/L-L-L phases, clearly indicating that, when  $\alpha$  and  $\mu$  are held constant, the phase boundary follows a nonmonotonic pattern with respect to  $\beta$ . This causes the phase boundary to take a turn around as can be seen in Fig. 3(d). To illustrate these transitions in detail, we have plotted Fig. 7 to display various density profiles while keeping  $\alpha = 4$ ,  $\mu = 0.7$ , and employing different values of  $\beta$ . The unusual behavior of the system can be elucidated through the following intuitive explanation. When we fix  $\alpha = 4$ , initially increasing  $\beta$  results in a raised exit rate for both species of particles from their respective output lane. Consequently,

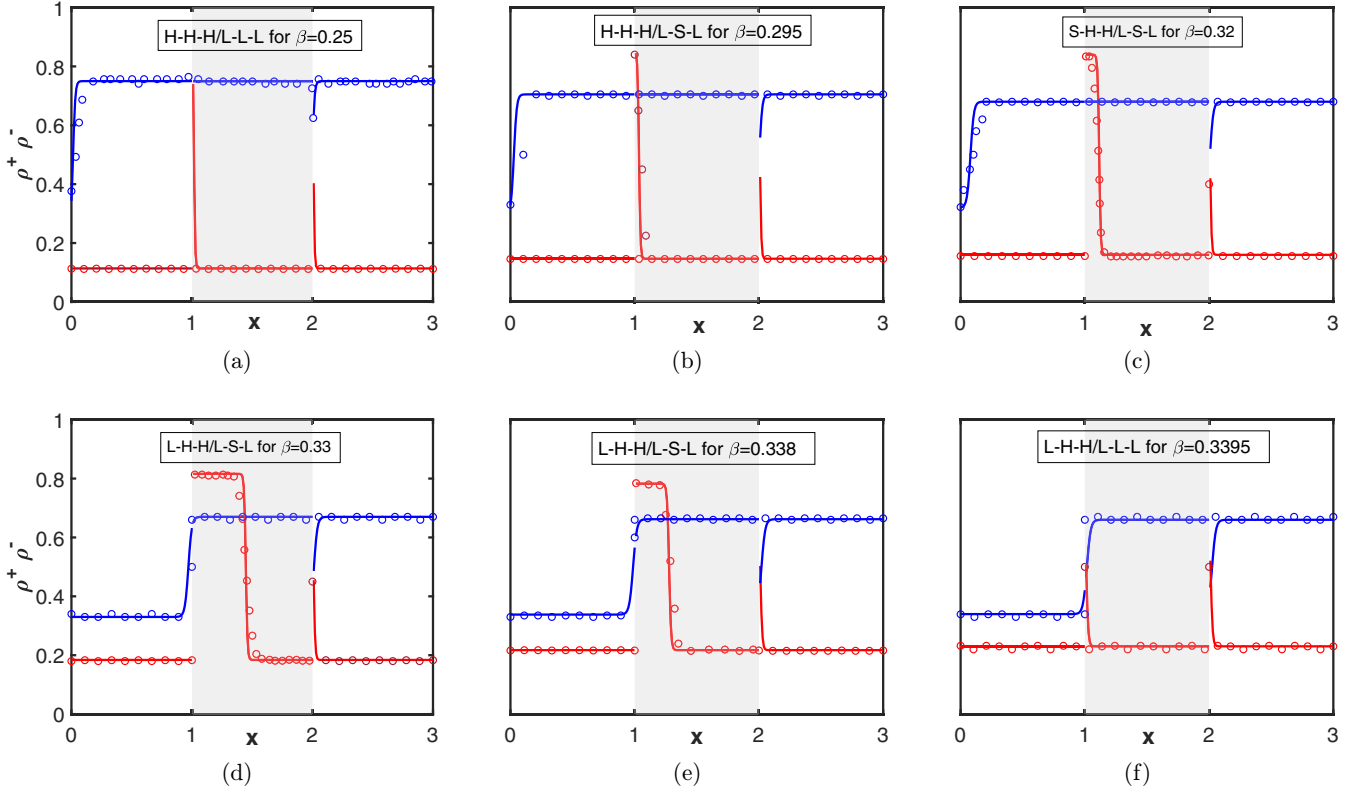


FIG. 6. Dynamics of the phase involving shock for  $\mu = 0.7$ ,  $\alpha = 12$  and different values of  $\beta$ . (a)  $\rightarrow$  (b)  $\rightarrow$  (c)  $\rightarrow$  (d)  $\rightarrow$  (e)  $\rightarrow$  (f) gives the order of the phase transition. Solid lines give mean-field results while symbols correspond to Monte Carlo simulations. The shaded region for  $x \in [1, 2]$  represents the bridge lanes.

a greater number of particles become available in the pool to be pushed onto the lanes. This leads to an enhancement in the modified entrance rates, i.e.,  $\alpha_{in,eff}^{\pm}$ , for the two species of particles. As a result, the positive species starts accumulating on lane P, causing a hindrance to the exit of the negative species. This accumulation gives rise to a shock in lane P for the positive species, which moves toward the left as  $\beta$  continues to increase. During this stage, the system maintains equal entrance-exit rates in lane P for the positive species, but this equilibrium is disrupted as  $\beta$  further increases. Eventually, the shock reaches the left end, causing a phase transition from S-H-H/L-L-L to H-H-H/L-L-L at the critical value of  $\beta = 0.1063$ . Subsequently, the entrance rate of the positive species onto lane P remains higher than the exit rate from lane P, as confirmed by the theoretical Eq. (B2). The modified entrance rate  $\alpha_{in,eff}^+$  is a diminishing slope function of  $\beta$ , which eventually reaches the value  $\beta_{in}^+$ . At the critical value of  $\beta = 0.2764$ , the system once again exhibits the S-H-H/L-L-L configuration.

Similarly, the phase diagram depicted in Fig. 3(e) also illustrates a recurring pattern of transitions. It begins with a movement from the symmetric HD-HD-LD/HD-HD-LD and the asymmetric L-L-L/L-L-L phases, followed by a shift to the symmetric LD-LD-LD/LD-LD-LD phase, and ultimately returning to the HD-HD-LD/HD-HD-LD phase. This progression can be explained as follows:

Consider the case where  $\alpha = 1$  and  $\mu$  tend toward infinity. In situations where resources are abundant, the entrance rate

through the input lane remains fixed and is represented by the parameter  $\alpha$ , which is smaller than  $\beta$  in this scenario. Consequently, a greater number of particles enter the system than exit, resulting in an accumulation of particles in the input and bridge lane, which leads to the HD-HD-LD/HD-HD-LD phase where the system shows a 1-1-0 density profile for each of the particle species.

However, as the value of  $\beta$  increases, more particles start leaving through the output lanes. This leads to a transition toward the L-L-L/L-L-L phase, and subsequently to the LD-LD-LD/LD-LD-LD phase. In the case of larger values of  $\beta$ , the increased particle exit rate from the output lane causes a low-density phase to emerge in this lane. As a result, the other lanes experience a high-density phase. If one considers the particle density as the order parameter, then these transitions are of first order.

**D. Finite-size effect**

The exploration of the TASEP model incorporating bidirectional dynamics has provided insights into the impact of finite system size on the asymmetric low-density phase. In our study, the asymmetric phase, L-L-L/L-L-L, emerges even at extremely small values of the filling factor  $\mu$  and continues to persist as  $\mu$  increases. Based on the theoretical investigation revealed by the mean-field framework, it has been observed that this phase remains confined to a curve in the phase plane as shown in Fig. 3. However, numerical

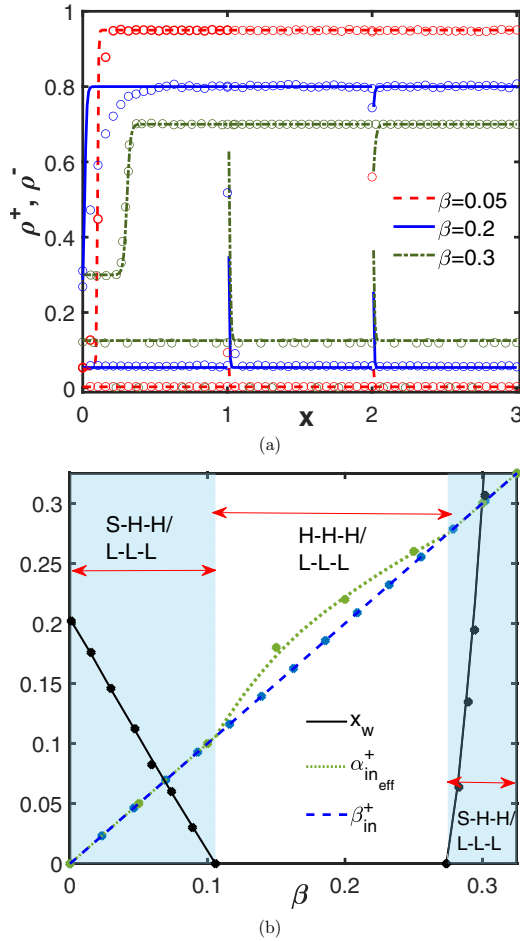


FIG. 7. (a) Density profiles displaying back-and-forth transition for  $\mu = 0.7$  and  $\alpha = 4$  with  $\beta = 0.05$  (S-H-H/L-L-L),  $0.2$  (H-H-H/L-L-L), and  $0.3$  (S-H-H/L-L-L). (b) Effective entry-exit rates and the position of shock  $x_w$  [given by Eq. (B6)] of the positive particles for lane P for fixed  $\mu = 0.7$  and  $\alpha = 4$ . Solid lines denote theoretical results and round symbols show Monte Carlo simulation results.

simulations conducted using the Gillespie Algorithm for  $N = 100$  demonstrate that this phase exists over a substantial region, rather than just a curve. Nevertheless, as the lattice length of each lane increases, the region encompassing this asymmetric phase shrinks, suggesting its disappearance in the thermodynamic limit and validating the theoretical findings. To examine this effect caused by finite lane size, we plot the region width  $\Delta$  with respect to  $\beta$  of the L-L-L/L-L-L region displayed by the system while keeping  $\alpha = 0.4$  and  $\mu = 0.45$ , as illustrated in Fig. 8. As observed from the figure, the width of the L-L-L/L-L-L region decreases as the size of each lane, denoted by  $N$ , increases. Therefore, for sufficiently large systems, the observed region contracts, which aligns with our theoretical observations. It is important to mention that the size of the symbols depicted in Fig. 3 representing the simulation results have been appropriately chosen to reflect the impact of finite lane length.

The theoretical analysis of our model heavily relies on the assumption of a thermodynamic limit, where the number of sites in each lane ( $N$ ) tends to infinity. However, in Monte

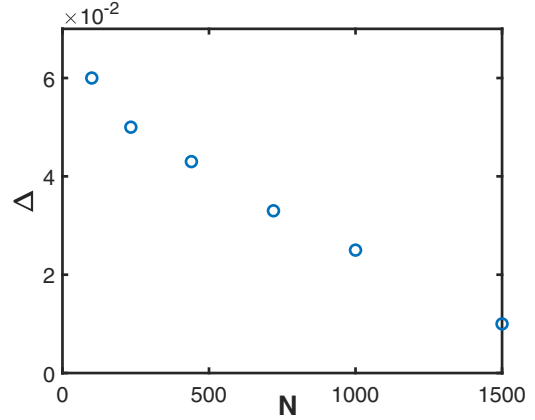


FIG. 8. Variation of region width  $\Delta$  of L-L-L/L-L-L phase with increasing  $\beta$  for fixed  $\alpha = 0.4$  and  $\mu = 0.45$  obtained through simulations.

Carlo simulations, the length of each lane, denoted as  $N$ , is a finite value. This finite length effect is also noticeable in the boundary that separates the LD-SP-LD/LD-SP-LD phase from the SP-HD-LD/SP-HD-LD phase, which is identified as the LD-HD-LD/LD-HD-LD phase. It has been observed that as the value of  $N$  increases, the boundary predicted by the Monte Carlo simulations approaches the one obtained through theoretical analysis. In other words, we graph the position where this transition occurs for fixed values of  $\mu = 0.8$  and  $\beta = 0.9$  while increasing  $N$ . It is found that the deviation from the theoretically derived phase boundary decreases as  $N$  increases and for  $N \approx 3000$ , this deviation approaches the value obtained analytically (Fig. 9). Beyond this point, no further changes are observed in this position. A similar effect can be witnessed in the phase boundary between LD-SP-LD/LD-SP-LD and HD-HD-LD/HD-HD-LD phase. Thus we have refrained from plotting these phase boundaries through MCs in the phase diagram given by Fig. 3.

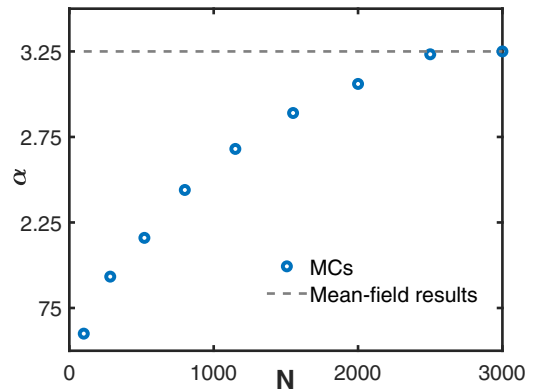


FIG. 9. Variation of phase boundary separating LD-SP-LD/LD-SP-LD region from SP-HD-LD/SP-HD-LD region for  $\beta = 0.9$  and  $\mu = 0.8$ . The MCs results (symbols) approach the boundary obtained through a theoretical framework (dotted line) for larger values of  $N$ .

## VI. CONCLUSION

In this paper, we study a particular variant of the exclusion model about roundabouts, consisting of two bridge lanes in the middle with particles traveling in opposite directions. These bridge lanes are intricately linked to a bidirectional TASEP lane on each side. A global constraint on the total number of particles in the system is considered and is characterized by a filling factor. The interactions of the bridge lanes with the side lane induce an inhomogeneity in the system which is dealt with by defining appropriate effective entrance and exit rates. Mean-field approximations are employed to calculate critical stationary characteristics, such as phase diagrams, significant density profiles, and phase transitions, to comprehend the impact of finite resources on the system dynamics. The theoretical findings are validated through dynamic Monte Carlo simulations performed by utilizing the Gillespie Algorithm.

The main goal of our theoretical analysis is to probe the effect of coupling the system to a finite pool on the spontaneous symmetry-breaking phenomenon. With an increase in the particle count, significant qualitative and quantitative changes are observed in the phase diagram. The exact location of the phases, the phase boundaries as well as the density profiles are governed by the entrance and exit rates from the extreme ends in addition to the filling factor. The complexity of the phase diagram is highly sensitive to the filling factor  $\mu$  which controls the number of resources in the system. Though the phase diagram is comparatively simplified for smaller and larger values of  $\mu$ , but for intermediate values the complexity is enhanced. This leads to a nonmonotonic variation in the number of phases portrayed with increasing  $\mu$ . Moreover, we found two congested phases where the particles are stuck in a jammed state and no further movement is possible. The most striking property of the proposed study is the advent of a back-and-forth phase transition which exists even when there is no scarcity of particles available to the lanes. In addition to this, the system attains phases that display boundary-induced shock corresponding to one and bulk-induced shock with respect to the other particle species. To obtain insight into the nature of transitions across the phase boundaries, we have considered the position of shock as the order parameter. We present explicit calculations for phase boundaries and density profiles in both symmetric and asymmetric phases. Furthermore, we offer straightforward physical explanations to elucidate the theoretical observations.

The present work is an attempt to understand the complex nonequilibrium bidirectional transportation of particles on roundabout like structure in a constrained environment. Our model effectively captures crucial aspects of bidirectional transport observed in scenarios involving biological molecular motors and vehicular traffic on roundabout-like network configurations. It serves as a valuable tool for controlling and managing transport mechanisms within network models, offering efficiency through the adjustment of boundary-controlling parameters and resource availability. This capability holds significant promise in improving the design and operation of transportation systems, communication networks, and other systems where efficient and controlled transport is essential for their functionality and performance.

The theoretical framework is not only limited to intracellular traffic by motor proteins or vehicular traffic, but can also be generalized for any kind of system where bidirectional transport takes place along junctions. In the future, this study can be extended to incorporate different features such as dynamic defects, interactions between entities, Langmuir Kinetics, etc.

## ACKNOWLEDGMENTS

The first author thanks the Council of Scientific and Industrial Research (CSIR), India for financial support under File No. 09/1005(0023)/2018-EMR-I. A.K.G. acknowledges support from DST-SERB, Government of India (Grant No. CRG/2019/004669). This work was partially supported by the FIST program of the Department of Science and Technology, Government of India, Reference No. SR/FST/MS-I/2018/22(C).

## APPENDIX A: SYMMETRIC PHASES

### 1. LD-LD-LD/LD-LD-LD phase

In this phase, both the particle species display a low-density phase in all the lanes. Each lane is entry-dominated and the corresponding particle density is equal to the effective entrance rates of the respective lanes. So, the bulk and the boundary densities of each lane is given by

$$\begin{aligned} \rho_{\text{in}}^1 &= \alpha_{\text{in,eff}}, & \rho_{\text{in}} &= \alpha_{\text{in,eff}}, & \rho_{\text{in}}^{+,N} &= \frac{J_{\text{in}}}{\beta_{\text{in}}}, \\ \rho_B^{+,1} &= \alpha_B, & \rho_B &= \alpha_B, & \rho_B^{+,N} &= \frac{J_B}{\beta_B}, \\ \rho_{\text{out}}^{+,1} &= \alpha_{\text{out,eff}}, & \rho_{\text{out}} &= \alpha_{\text{out,eff}}, & \rho_{\text{out}}^N &= \frac{J_{\text{out}}}{\beta}. \end{aligned}$$

The bulk currents in each lane is given by

$$\begin{aligned} J_{\text{in}} &= \alpha_{\text{in,eff}}(1 - \alpha_{\text{in,eff}}), \\ J_B &= \alpha_B(1 - \alpha_B), \\ J_{\text{out}} &= \alpha_{\text{out,eff}}(1 - \alpha_{\text{out,eff}}). \end{aligned} \tag{A1}$$

Necessary conditions for the existence of this phase are given by

$$\begin{aligned} \alpha_{\text{in,eff}} &< \min\{\beta_{\text{in}}, 0.5\}, & \alpha_B &< \min\{\beta_B, 0.5\}, \\ \alpha_{\text{out,eff}} &< \min\{\beta, 0.5\}. \end{aligned}$$

Inserting the boundary as well as bulk densities stated above in Eqs. (9), (11), and (19) to obtain

$$\begin{aligned} \alpha_{\text{in,eff}} &= \alpha_{\text{out,eff}} = \frac{\alpha^* \beta}{\alpha^* + \beta}, \\ \beta_{\text{in}} &= 1 - \alpha_B, \\ \alpha_B &= \alpha_{\text{in,eff}}, \\ \beta_B &= 1 - \alpha_{\text{out,eff}} - \alpha_{\text{in,eff}}. \end{aligned}$$

All these above-attained expressions for the effective entrance and exit rates when plugged in Eq. (23) yields

$$\mu = r + \frac{6}{4} \alpha_{\text{in,eff}},$$

which provides us with the pool capacity as

$$r = \frac{1}{4\alpha} [2\mu(\alpha - \beta) - 3\alpha\beta + \sqrt{16\alpha\beta\mu^2 + (2\mu(\alpha - \beta) - 3\alpha\beta)^2}].$$

Under these circumstances, the existential condition for this phase is

$$\alpha_{\text{in,eff}} < \beta_B. \quad (\text{A2})$$

## 2. HD-HD-LD/HD-HD-LD phase

We assume that in this symmetric phase both the particle species manifest high-density phase in their input as well as bridge lanes while the output lane displays LD phase. The specifications that support the extant of this asymmetric phase are

$$\begin{aligned} \rho_{\text{in}} &= 1 - \beta_{\text{in}}, \\ \rho_B &= 1 - \beta_B, \\ \rho_{\text{out}} &= \alpha_{\text{out,eff}}. \end{aligned}$$

One solves Eqs. (9) and (19) to get

$$\beta_B = \beta_{\text{in}} = 1 - \alpha_B, \quad \alpha_{\text{out,eff}} = 0.$$

Physically it implies that the density of positive species in lane Q given by  $\alpha_{\text{out,eff}}$  is 0. This means that there is no particle movement from the bridge onto lane Q, suggesting that  $\beta_{\text{in}} = \beta_B = 0$ . Thus, we have that, the particle density in the input as well as the bridge is 1 while in the output lane, it is 0. As particle movement is not possible in this scenario, this phase can also be referred to as a congested phase.

Utilizing the particle number conservation given by Eq. (23), we have  $r = \mu - 1$ . So, it is evident that the HD-HD-LD/HD-HD-LD phase persists only when  $\mu > 1$  and continues to exist as  $\mu \rightarrow \infty$ . As the particle density is independent of the boundary-controlling parameters, the phase boundaries for this region can only be calculated numerically.

## 3. LD-SP-LD/LD-SP-LD

The particle density, in this case, displays a constant density of  $\alpha_{\text{in,eff}}$  in the input lanes, a shock in the bridge lanes where a constant density of  $\alpha_B$  is connected to density  $1 - \beta_B$  on the right and again low-density phase in the output lanes with density  $\alpha_{\text{out,eff}}$ . In this case, one can compute the relation between the rates as

$$\begin{aligned} \alpha_B &= \alpha_{\text{in,eff}}, \\ \alpha_{\text{out}} &= 1 - \beta_B, \\ \beta_{\text{in}} &= 1 - \alpha_B, \\ \beta_B &= 1 - \alpha_{\text{out,eff}} - \alpha_B. \end{aligned}$$

Utilizing the above equations to solve Eqs. (15) and (16) gives

$$\begin{aligned} \alpha_{\text{in,eff}} &= \frac{\alpha^*(4\beta - 1)}{\alpha^* + 4\beta}, \\ \alpha_{\text{out,eff}} &= \frac{\alpha^* + 2\beta(1 - \alpha^*)}{\alpha^* + 4\beta}. \end{aligned}$$

Since the existence of the shock phase in the bridge lane requires  $\alpha_B = \beta_B$ , we obtain the capacity of the pool as

$$r = \frac{\beta\mu}{\alpha(3\beta - 1)}.$$

To calculate the position of the shock  $x_w$ , one needs to solve the Eq. (23), which gives

$$x_w = \frac{6\beta\mu - 2\alpha(3\beta - 1)(3\mu - 2)}{\alpha(3\beta - 1)}. \quad (\text{A3})$$

Thus, one can write the existential condition for this phase as

$$0 < x_w < 1. \quad (\text{A4})$$

## 4. SP-HD-LD/SP-HD-LD

In this case, Eqs. (11), (9), and (19) reduces to

$$\begin{aligned} \alpha_B &= 1 - \beta_{\text{in}}, \\ \beta_B &= 1 - \alpha_{\text{out,eff}} - \alpha_B, \\ \alpha_{\text{out}} &= 1 - \beta_B, \\ \beta_{\text{in}} &= \frac{\beta_B(1 - \beta_B)}{\alpha_B}, \end{aligned}$$

along with the modified entrance rates given by

$$\begin{aligned} \alpha_{\text{in,eff}} &= \frac{\alpha_{\text{in,eff}}(1 - \alpha_{\text{in,eff}})}{\frac{\alpha_{\text{in,eff}}(1 - \alpha_{\text{in,eff}})}{\alpha^*} + \frac{\alpha_{\text{out,eff}}(1 - \alpha_{\text{out,eff}})}{\beta}}, \\ \alpha_{\text{out,eff}} &= \frac{\alpha_{\text{out,eff}}(1 - \alpha_{\text{out,eff}})}{\frac{\alpha_{\text{out,eff}}(1 - \alpha_{\text{out,eff}})}{\alpha_{\text{out}}} + \frac{\beta_{\text{in}}(1 - \beta_{\text{in}})}{\beta_{\text{in}}}}. \end{aligned}$$

From the above equations, we can deduce that  $\beta_{\text{in}} = \beta_B$  which further implies that  $\alpha_{\text{out,eff}} = 0$ . This indicates that the entrance of particles to the output lane is restrained, forcing the exit rate  $\beta_B$  from the bridge lane to take the value 0. As  $\beta_{\text{in}} = \beta_B = \alpha_{\text{out,eff}} = 0$ , there are no positive particles in the output lane while the bridge lane is fully packed with particle density 1. Now, the input lanes display a shock phase where a density profile connects a region of low-density to high-density region with particle density changing from  $\alpha_{\text{in,eff}}$  to  $1 - \beta_{\text{in}}$ . The existence of this phase requires  $\alpha_{\text{in,eff}}$  to remain equal to  $\beta_{\text{in}}$ , which implies that  $\alpha_{\text{in,eff}} = 0$ . Last, one can obtain the existential criteria for this phase numerically. As particle movement is not possible in this scenario, this phase is also referred to as a congested phase.

## APPENDIX B: ASYMMETRIC PHASES

### 1. L-L-L/L-L-L phase

During the L-L-L/L-L-L phase, all lanes experience a low-density phase, but the current and bulk density differ between the two types of particles. Upon calculating the effective rates for each lane, they are found to satisfy a simple relation expressed as

$$\alpha_{\text{in,eff}}^+ = \alpha_B^+ = \alpha_{\text{out,eff}}^+ = 1 - \beta_{\text{in}}^+ = 1 - \beta_B^+ + \alpha_{\text{in,eff}}^-,$$

along with

$$\alpha_{\text{in,eff}}^- = \alpha_B^- = \alpha_{\text{out,eff}}^- = 1 - \beta_{\text{in}}^- = 1 - \beta_B^- + \alpha_{\text{in,eff}}^+.$$

Here,  $\alpha_{\text{in,eff}}^+$  and  $\alpha_{\text{in,eff}}^-$  are obtained by solving Eqs. (15) and (16) as

$$\alpha_{\text{in,eff}}^+ = \frac{1}{2(\alpha^* - \beta)^2(\alpha^* + \beta)} \{ \beta^3 + \alpha^*(\beta - 1)[\beta^2 - (\alpha^*)^2] - (\alpha^*)^2\beta \pm \sqrt{(\alpha^* - \beta)^2[\beta^4 + 2(\alpha^*)^3(1 - \beta)\beta^2 - 2\alpha^*\beta^4 + (\alpha^*)^4(1 - 2\beta - 3\beta^2) + (\alpha^*)^2\beta^2(\beta^2 + 2\beta - 2)]} \}. \quad (\text{B1})$$

The above expressions are used to determine the pool capacity as

$$r = \frac{1}{8\alpha} \{ 4\mu(\alpha + \beta) + 3\alpha(\beta - 1) + \sqrt{16\alpha\beta(3 - 4\mu)\mu + [4\beta\mu + \alpha(4\mu + 3\beta - 3)]^2} \}.$$

Thus, the constraint on the parameters to attain this phase is

$$\alpha_{\text{out,eff}}^- < \beta.$$

## 2. H-H-H/L-L-L Phase

In this phase, the positive species portray the HD phase while the negative species display the entrance dominant phase in all the lanes. In such a scenario, the bulk currents are given by

$$\begin{aligned} J_{\text{in}}^+ &= \beta_{\text{in}}^+(1 - \beta_{\text{in}}^+), \\ J_B^+ &= \beta_B^+(1 - \beta_B^+), \\ J_{\text{out}}^+ &= \beta(1 - \beta), \\ J_{\text{in}}^- &= \alpha_{\text{in,eff}}^-(1 - \alpha_{\text{in,eff}}^-), \\ J_B^- &= \alpha_B^-(1 - \alpha_B^-), \\ J_{\text{out}}^- &= \alpha_{\text{out,eff}}^-(1 - \alpha_{\text{out,eff}}^-), \end{aligned}$$

which assists us in writing the boundary densities for each lane as

$$\begin{aligned} \rho_{\text{in}}^{+,1} &= 1 - \frac{J_{\text{in}}^+}{\alpha_{\text{in,eff}}^+}, & \rho_{\text{in}}^{+,N} &= 1 - \beta_{\text{in}}^+, \\ \rho_B^{+,1} &= 1 - \frac{J_B^+}{\alpha_B^+}, & \rho_B^{+,N} &= 1 - \beta_B^+, \\ \rho_{\text{out}}^{+,1} &= 1 - \frac{J_{\text{out}}^+}{\alpha_{\text{out,eff}}^+}, & \rho_{\text{out}}^{+,N} &= 1 - \beta, \\ \rho_{\text{in}}^{-,1} &= \frac{J_{\text{in}}^-}{\beta_{\text{in}}^-}, & \rho_{\text{in}}^{-,N} &= \alpha_{\text{in,eff}}^-, \end{aligned}$$

$$r = \frac{\{3\alpha(4\mu - 3) + 4\mu(6\beta + 8\mu - 9) + 3\sqrt{\alpha^2(3 - 4\mu)^2 + 16\mu^2 - 8\alpha\mu[3 + 6\beta^2 - 4\mu + 4\beta(2\mu - 3)]}\}}{8(3\alpha + 4\mu)}.$$

Thus, one can identify the relevant region for this phase as

$$\alpha_{\text{in,eff}}^- + \alpha_{\text{out,eff}}^- \leq \beta \leq \alpha_{\text{in,eff}}^+. \quad (\text{B3})$$

$$\rho_{\text{out}}^{-,1} = \frac{J_{\text{out}}^-}{\beta}, \quad \rho_{\text{out}}^{-,N} = \alpha_{\text{out,eff}}^-,$$

$$\rho_B^{-,1} = \frac{J_B^-}{\beta_B^-}, \quad \rho_B^{-,N} = \alpha_B^-.$$

Again one can solve Eqs. (9), (11), and (19) along with Eqs. (15) and (16) to obtain the values of the effective entrance and exit rates for the positive species as

$$\begin{aligned} \beta_B^+ &= 1 - \alpha_{\text{out}}^+ = 1 - \alpha_B^+ = \beta_{\text{in}}^+ = \beta, \\ \alpha_{\text{out,eff}}^+ &= \frac{\beta(1 - \beta)}{\beta + \alpha_{\text{in,eff}}^-}, \\ \alpha_{\text{in,eff}}^+ &= \frac{\beta(1 - \beta)}{\frac{\mu\beta(1 - \beta)}{\alpha r} + \frac{\alpha_{\text{out,eff}}^-(1 - \alpha_{\text{out,eff}}^-)}{\beta}}, \end{aligned} \quad (\text{B2})$$

while for the negative species,

$$\begin{aligned} \alpha_B^- &= 1 - \beta_{\text{in}}^- = \alpha_{\text{in,eff}}^-, \\ \alpha_{\text{in,eff}}^- &= \frac{1}{2}((1 + \alpha^*) - \sqrt{(1 + \alpha^*)^2 - 4\alpha^*\beta}), \\ \alpha_{\text{out}}^- &= \frac{\alpha_{\text{in,eff}}^-(1 - \alpha_{\text{in,eff}}^-)}{\beta - \alpha_{\text{in,eff}}^-}, \\ \alpha_{\text{out,eff}}^- &= \frac{((1 + \alpha_{\text{out}}^-) - \sqrt{(1 + \alpha_{\text{out}}^-)^2 - 4\alpha_{\text{out}}^-\beta})}{2}, \\ \beta_B^- &= \beta - \alpha_{\text{out,eff}}^-. \end{aligned}$$

Here, the equation for the pool dynamics given by Eq. (23) gets converted to

$$\mu = r + \frac{(3(1 - \beta) + 2\alpha_{\text{in,eff}}^- + \alpha_{\text{out,eff}}^-)}{4},$$

which gives the value of the pool capacity as

## 3. L-L-S/L-L-L phase

During this phase, we make an assumption that the (+) particles are in a low-density (LD) phase in lanes P and the

bridge, while lane Q exhibits a discontinuity in the density profile, connecting a region of low-density to high-density. However, the  $(-)$  particles represent a low-density phase in all the lanes. This phase persists when the boundary-controlling parameters satisfy the following conditions:

$$\begin{aligned}\alpha_{\text{in,eff}}^+ &< \min\{\beta_{\text{in}}^+, 0.5\}, & \alpha_{\text{in,eff}}^- &< \min\{\beta_{\text{in}}^-, 0.5\}, \\ \alpha_B^+ &< \min\{\beta_B^+, 0.5\}, & \alpha_B^- &< \min\{\beta_B^-, 0.5\}, \\ \alpha_{\text{out,eff}}^+ &= \beta < 0.5, & \alpha_{\text{out,eff}}^- &< \min\{\beta, 0.5\}.\end{aligned}$$

The effective boundary rates as retrieved from Eqs. (9), (11), and (19) is

$$\begin{aligned}\alpha_{\text{in,eff}}^+ &= \alpha_B^+, & \alpha_{\text{out}}^+ &= \frac{\alpha_{\text{in,eff}}^+ (1 - \alpha_{\text{in,eff}}^+)}{\beta_B^+}, \\ \alpha_{\text{in,eff}}^- &= \alpha_B^-, & \alpha_{\text{out}}^- &= \frac{\alpha_{\text{in,eff}}^- (1 - \alpha_{\text{in,eff}}^-)}{\beta_B^-},\end{aligned}$$

along with

$$\begin{aligned}\beta_B^+ &= 1 - \alpha_{\text{in,eff}}^- - \alpha_{\text{out,eff}}^+, \\ \beta_B^- &= 1 - \alpha_{\text{in,eff}}^+ - \alpha_{\text{out,eff}}^-.\end{aligned}$$

These values can now be substituted in Eqs. (15) and (16) to get

$$\begin{aligned}\alpha_{\text{in,eff}}^- &= \frac{(1 + \alpha^*) - \sqrt{(1 + \alpha^*)^2 - 4\alpha^*\beta}}{2}, \\ \alpha_{\text{in,eff}}^+ &= \frac{1}{2\beta} [\beta(1 + \alpha^*) \\ &\quad - \sqrt{\beta^2(1 - \alpha^*)^2 + 4\alpha_{\text{in,eff}}^- \alpha^* \beta (1 - \alpha_{\text{in,eff}}^-)}].\end{aligned}$$

Since the flow of particles is continuous throughout the system, we have  $\alpha_{\text{in,eff}}^+ = \alpha_B^+ = \alpha_{\text{out,eff}}^+$  and  $\alpha_{\text{in,eff}}^- = \alpha_B^- = \alpha_{\text{out,eff}}^-$ . To acquire the value of pool capacity, one can solve the condition that  $\alpha_{\text{out,eff}}^+ = \beta$  which is the requirement for lane Q to remain in the S phase for the positive species. Now, the only variable that is left to be calculated is  $x_w$ , the position of shock. Note that

$$\int_0^1 \rho_{\text{out}}^+ dx = \int_0^{x_w} \alpha_{\text{out,eff}}^+ dx + \int_{x_w}^1 (1 - \beta) dx,$$

and finally one can revisit Eq. (23) to obtain the value of the shock position as

$$x_w = \frac{4(\mu - r) - 3\alpha_{\text{in,eff}}^- - 2\alpha_{\text{in,eff}}^+ - 1 + \beta}{2\beta - 1}. \quad (\text{B4})$$

Thus, one needs to identify the region where Eq. (B3) as well as the condition  $0 < x_w < 1$  is obeyed. As  $x_w \rightarrow 1$ , we reach the L-L-L/L-L-L phase whereas when  $x_w$  takes the value 0, the shock position shifts toward the left end of lane Q and the system exhibits the L-L-H/L-L-L phase. In the limiting case of  $\mu \rightarrow \infty$ , this phase does not exist.

#### 4. L-L-H/L-L-L phase

The sole distinction between this phase and the L-L-S/L-L-L phase lies in the location of the shock within lane Q for the positive species. In the previous scenario, the shock had to

be positioned away from the boundaries, whereas in this case, the value of  $x_w$  needs to be precisely 0 to achieve the L-L-H/L-L-L phase. It is important to note that the L-L-H/L-L-L phase does not exist in the limit where  $\mu$  approaches infinity. Furthermore, this phase serves as a boundary that separates the region of L-L-S/L-L-L from the region of L-S-H/L-L-L.

#### 5. L-S-H/L-L-L phase

Once again, we follow a similar procedure as we did for the previous phases. The continuous flow of particles within the system implies that  $\alpha_{\text{in,eff}}^+ = \alpha_B^+$ ,  $\beta_B^+ = \beta$ , and  $\alpha_{\text{in,eff}}^- = \alpha_B^- = \alpha_{\text{out,eff}}^-$ . To determine the values of these modified entrance rates, we utilize Eqs. (15) and (16), resulting in

$$\begin{aligned}\alpha_{\text{in,eff}}^- &= \frac{1}{2} [(1 + \alpha^*) - \sqrt{(1 + \alpha^*)^2 - 4\alpha^*\beta}], \\ \alpha_{\text{in,eff}}^+ &= \frac{1}{2\beta} [\beta(1 + \alpha^*) \\ &\quad - \sqrt{\beta^2(1 - \alpha^*)^2 + 4\alpha_{\text{in,eff}}^- \alpha^* \beta (1 - \alpha_{\text{in,eff}}^-)}].\end{aligned} \quad (\text{B5})$$

By solving  $\alpha_B^+ = \beta_B$ , the necessary condition for the existence of S phase in the bridge lane, we can determine the pool capacity. Furthermore, the position of the shock can be obtained using Eq. (23) as

$$x_w = \frac{4(\mu - r) - 2(1 - \beta) - 3\alpha_{\text{in,eff}}^- - \alpha_{\text{in,eff}}^+}{\alpha_{\text{in,eff}}^+ + \beta - 1}.$$

When the value of  $x_w$  approaches 1, the system manifests the L-L-H/L-L-L phase. Conversely, as  $x_w$  tends to 0, L-H-H/L-L-L is attained. Additionally, this phase disappears as  $\mu$  approaches infinity.

#### 6. S-H-H/L-L-L phase

The continuous flow of particles leads to significant implications, particularly regarding the bulk densities of lane P, bridge, and Q. Specifically, the bulk density corresponding to the negative species is given by  $\alpha_{\text{in,eff}}^-$ , which remains consistent across all the three lanes. Similarly, for the positive species, we can establish the requirement that  $\beta_{\text{in}}^+ = \beta_B^+ = \beta$  to maintain a continuous flow. By utilizing these conditions in Eqs. (15) and (16) we obtain the following expressions:

$$\begin{aligned}\alpha_{\text{in,eff}}^- &= \frac{1}{2} [(1 + \alpha^*) - \sqrt{(1 + \alpha^*)^2 - 4\alpha^*\beta}], \\ \alpha_{\text{in,eff}}^+ &= \frac{1}{2\beta} [\beta(1 + \alpha^*) \\ &\quad - \sqrt{\beta^2(1 - \alpha^*)^2 + 4\alpha_{\text{in,eff}}^- \alpha^* \beta (1 - \alpha_{\text{in,eff}}^-)}].\end{aligned}$$

To acquire the capacity of the pool, one can solve  $\alpha_{\text{in,eff}}^+ = \beta$ . Additionally, the position of the shock can be calculated from Eq. (23) as

$$x_w = \frac{4(\mu - r) - 3(\alpha_{\text{in,eff}}^- + 1 - \beta)}{2\beta - 1}. \quad (\text{B6})$$

The region of existence for this phase can be expressed in a similar manner as demonstrated for other cases.

### 7. L-H-H/L-L-L phase

Here, the positive species display the LD phase in lane P while the other two lanes are in high-density phase whereas the negative species of all the lanes are in entrance dominated phase. Similar to the previous scenario, we can derive the following expressions:

$$\begin{aligned}\alpha_{\text{in,eff}}^- &= \frac{1}{2}[1 + \alpha^* + \sqrt{(1 + \alpha^*)^2 - 4\alpha^*\beta}], \\ \alpha_{\text{out,eff}}^- &= \alpha_{\text{in,eff}}^- = \alpha_B^-, \\ \alpha_{\text{in,eff}}^+ &= \frac{1}{2\beta}[\beta(1 + \alpha^*) \\ &\quad - \sqrt{\beta^2(1 - \alpha^*)^2 + 4\alpha_{\text{in,eff}}^- \alpha^* \beta(1 - \alpha_{\text{in,eff}}^-)}].\end{aligned}$$

The existence of this phase is determined by the position of  $x_w$  in S-H-H/L-L-L reaching the right boundary of lane P, specifically when  $x_w = 1$ . This condition defines the curve that represents the existence of this phase.

### 8. H-H-H/L-S-L phase

During this phase, the positive species display exit dominated phase in the input, bridge, and output lane, whereas the other species of particles are in entrance dominated phase in the input and output lane, with the bridge lane exhibiting a shock phase. The modified and effective entrance-exit rates for the different lanes can be derived similarly to the previous phase which provides us with

$$\begin{aligned}\alpha_{\text{in,eff}}^- &= \frac{1}{2}[1 + \alpha^* + \sqrt{(1 + \alpha^*)^2 - 4\alpha^*\beta}], \\ \alpha_{\text{out,eff}}^- &= \frac{\beta}{2}, \\ \alpha_{\text{out,eff}}^+ &= \frac{\beta(1 - \beta)}{\beta + \alpha_{\text{in,eff}}^-}, \\ \alpha_{\text{in,eff}}^+ &= \frac{8\alpha^2(1 - \beta)}{[4(1 - \beta) - \alpha^2](2 - \beta)}, \\ \beta_B^- &= \beta - \alpha_{\text{out,eff}}^-, \end{aligned}$$

along with the conditions  $\beta_{\text{in}}^+ = \beta_B^+ = \beta$ ,  $\alpha_{\text{in,eff}}^- = \alpha_B^-$ . The condition for the existence of the shock phase in the bridge lane corresponding to the negative species,  $\alpha_B^- = \beta_B^-$ , is utilized to determine the pool capacity and is given by

$$r = \frac{\mu(2 - \beta)}{2\alpha}. \quad (\text{B7})$$

The position of the shock can be determined from Eq. (23) as

$$x_w = \frac{8(\mu - r - 1) + 5\beta}{2(\beta - 1)}.$$

Thus, the necessary condition for the existence of this phase can be written as

$$0 < x_w < 1, \quad \beta < \min\{\alpha_{\text{out,eff}}^+, \alpha_{\text{in,eff}}^-\}.$$

This phase no longer exists in the limiting case of  $\mu$  tends to infinity.

### 9. H-H-H/L-H-L phase

The main distinction between this phase and the H-H-H/L-S-L phase is the specific location of the shock within the bridge lane for the negative species. Unlike the previous scenario where the shock needed to be positioned away from the boundaries; the value of  $x_w$  in the H-H-H/L-S-L must be precisely 0 for the system to achieve the H-H-H/L-H-L phase. As  $\mu$  tends toward infinity, the H-H-H/L-H-L phase becomes nonexistent.

### 10. S-H-H/L-S-L phase

The same analytical approach can be employed for this phase as in the other cases. However, due to the limited number of equations available, it is not possible to calculate the exact location of the shock or derive an explicit formulation for the phase boundaries.

### 11. S-H-H/L-H-L phase

In this phase, the effective entrance and exit rates can be obtained analogously as done for the S-H-H/L-L-L phase. These expressions can further be utilized to calculate the position of the shock as well as the pool capacity.

## APPENDIX C: DISCARDED PHASES

(i) The total particle density of the bidirectional lanes cannot be greater than one, i.e.,  $\rho_{\text{in}}^+ + \rho_{\text{out}}^- \not\leq 1$  and  $\rho_{\text{out}}^+ + \rho_{\text{in}}^- \not\leq 1$ . So, all the phases of the form  $X_1 - X_2 - X_3/Y_1 - Y_2 - Y_3$  where  $X_1, Y_3 \in \{\text{H/HD, S/SP, M/MC}\}$  cannot persist.

(ii) If  $X_1 \in \{\text{LD/L, HD/H}\}$ , then  $X_2 \neq \text{MC/M}$ .

(iii) If  $X_1 = \text{MC/M}$ , then  $X_2 \notin \{\text{LD/L, HD/H, MC/M}\}$ .

(iv) The remaining phases pose a challenge when attempting to evaluate Eqs. (9), (11), (19), as well as Eqs. (15) and (16), as their simultaneous resolution leads to a state of self-inconsistency.

## APPENDIX D: ALTERNATIVE APPROACH TO OBTAIN A DENSITY PROFILE

In this section, we present a numerical technique for acquiring density profiles for the proposed system. The continuum version of the evolution equation given by Eq. (5) is discretization through a finite difference scheme, wherein the time and space derivatives are substituted with forward and central difference formulas, respectively. By selecting spatial grid size  $\Delta x = 1/N$  and suitable time step  $\Delta t$  that satisfies the stability condition  $\Delta t/\Delta x^2 \leq 1$ , the solution is obtained as the limit  $n$  approaches infinity, where  $n$  is the number of time steps, ensuring the attainment of a steady state. The resulting

decoupled discretized equation is expressed as follows:

$$\begin{aligned}\rho_{j,i}^{+,n+1} &= \rho_{j,i}^{+,n} + \frac{\epsilon \Delta t}{2} \left( \frac{\rho_{j,i+1}^{+,n} - 2\rho_{j,i}^{+,n} + \rho_{j,i-1}^{+,n}}{\Delta x^2} \right) \\ &\quad + \Delta t \left( \frac{\rho_{j,i+1}^{+,n} - \rho_{j,i-1}^{+,n}}{2\Delta x} \right) (2\rho_{j,i}^{+,n} - 1), \\ \rho_{j,i}^{-,n+1} &= \rho_{j,i}^{-,n} + \frac{\epsilon \Delta t}{2} \left( \frac{\rho_{j,i+1}^{-,n} - 2\rho_{j,i}^{-,n} + \rho_{j,i-1}^{-,n}}{\Delta x^2} \right) \\ &\quad - \Delta t \left( \frac{\rho_{j,i+1}^{-,n} - \rho_{j,i-1}^{-,n}}{2\Delta x} \right) (2\rho_{j,i}^{-,n} - 1),\end{aligned}$$

where  $j$  takes the values 1, 2, and 3 to represent the input, bridge, and output lanes, respectively, and  $i \neq 1, N$ . As per our model, the lanes interact effectively at the boundary sites only. Hence, this effect is implemented by employing the mean-field version of the boundary equations for the (+) species as

$$\begin{aligned}\rho_{1,1}^{+,n+1} &= \rho_{1,1}^{+,n} + \Delta t \left[ \alpha \left( 1 - \frac{\sum_j \sum_i (\rho_{j,i}^{+,n} + \rho_{j,i}^{-,n})}{4N\mu} \right) \right. \\ &\quad \left. \times (1 - \rho_{1,1}^{+,n} - \rho_{1,1}^{-,n}) - \rho_{1,1}^{+,n}(1 - \rho_{1,2}^{+,n}) \right], \\ \rho_{1,N}^{+,n+1} &= \rho_{1,N}^{+,n} + \Delta t [\rho_{1,N-1}^{+,n}(1 - \rho_{1,N}^{+,n} - \rho_{1,N}^{-,n}) \\ &\quad - \rho_{1,N}^{+,n}(1 - \rho_{2,1}^{+,n})], \\ \rho_{2,1}^{+,n+1} &= \rho_{2,1}^{+,n} + \Delta t [\rho_{1,N}^{+,n}(1 - \rho_{2,1}^{+,n}) - \rho_{2,1}^{+,n}(1 - \rho_{2,2}^{+,n})], \\ \rho_{2,N}^{+,n+1} &= \rho_{2,N}^{+,n} + \Delta t [\rho_{2,N-1}^{+,n}(1 - \rho_{2,N}^{+,n}) \\ &\quad - \rho_{2,N}^{+,n}(1 - \rho_{3,1}^{+,n} - \rho_{3,1}^{-,n})], \\ \rho_{3,1}^{+,n+1} &= \rho_{3,1}^{+,n} + \Delta t [\rho_{2,N}^{+,n}(1 - \rho_{3,1}^{+,n} - \rho_{3,1}^{-,n})\end{aligned}$$

$$- \rho_{3,1}^{+,n}(1 - \rho_{3,2}^{+,n} - \rho_{3,2}^{-,n})],$$

$$\rho_{3,N}^{+,n+1} = \rho_{3,N}^{+,n} + \Delta t [\rho_{3,N-1}^{+,n}(1 - \rho_{3,N}^{+,n}) - \beta \rho_{3,N}^{+,n}].$$

Analogous equations can be written for the other species as well.

## APPENDIX E: MONTE CARLO SIMULATIONS

To conduct simulations, we utilize the Gillespie Algorithm within a Monte Carlo framework, implementing a random sequential update rule. At each time step, a site is selected based on a generated random number, and its state is updated according to the specific dynamical rules.

The occurrence of an event, such as a particle entering the input lane, particle hopping in the bulk, particle exiting the output lane, or species exchange, is determined probabilistically. The probability of selecting a particular event is proportional to the sum of all rates associated with that event. The time interval until the next event, denoted as  $\Delta t$ , follows an exponential distribution. In each simulation, the length of each lane is taken to be 1500. The typical run of each simulation is  $10^{10}$  time steps, with the initial 5% of observations discarded to ensure that the system has reached a stationary state before data are taken. In the case of large  $\alpha$ , it is necessary to discard the initial 20% of the simulations. Then, the observable quantities are recorded at every  $10N$  time step and averaged until the simulation terminates.

To construct phase diagrams through simulations, we measure the particle density and the current as a function of  $\alpha$  and  $\beta$ . These particle density values serve as an order parameter, allowing us to distinguish between different phases within the system. By varying these rates during simulations, we can construct a phase diagram that highlights distinct regions representing various phases. Determining the boundaries between these phases involves manually identifying specific values of  $\alpha$  and  $\beta$  at which the order parameter undergoes abrupt changes. Through simulations, these phase boundaries are plotted with an accuracy of under 2%, which is taken care of by the size of the circular symbols used in the plots.

- 
- [1] A. Schadschneider, D. Chowdhury, and K. Nishinari, *Stochastic Transport in Complex Systems: From Molecules to Vehicles* (Elsevier, Amsterdam, 2010).
- [2] T. Chou, K. Mallick, and R. K. Zia, *Rep. Prog. Phys.* **74**, 116601 (2011).
- [3] D. Chowdhury, *Phys. Rep.* **529**, 1 (2013).
- [4] B. Derrida, *Phys. Rep.* **301**, 65 (1998).
- [5] J. Krug, *Phys. Rev. Lett.* **67**, 1882 (1991).
- [6] A. Gupta, B. Pal, A. Jindal, N. Bhatia, and A. K. Gupta, *MethodsX* **10**, 101966 (2023).
- [7] C. T. MacDonald, J. H. Gibbs, and A. C. Pipkin, *Biopolymers: Original Res. Biomolecules* **6**, 1 (1968).
- [8] L. B. Shaw, R. K. P. Zia, and K. H. Lee, *Phys. Rev. E* **68**, 021910 (2003).
- [9] L. B. Shaw, A. B. Kolomeisky, and K. H. Lee, *J. Phys. A: Math. Gen.* **37**, 2105 (2004).
- [10] T. Chou and G. Lakatos, *Phys. Rev. Lett.* **93**, 198101 (2004).
- [11] T. Chou and D. Lohse, *Phys. Rev. Lett.* **82**, 3552 (1999).
- [12] S. Klumpp, T. M. Nieuwenhuizen, and R. Lipowsky, *Physica E* **29**, 380 (2005).
- [13] K. Nishinari, Y. Okada, A. Schadschneider, and D. Chowdhury, *Phys. Rev. Lett.* **95**, 118101 (2005).
- [14] D. Chowdhury, L. Santen, and A. Schadschneider, *Phys. Rep.* **329**, 199 (2000).
- [15] M. E. Froulaadvand and P. Maass, *Phys. Rev. E* **94**, 012304 (2016).
- [16] M. R. Evans, D. P. Foster, C. Godrèche, and D. Mukamel, *J. Stat. Phys.* **80**, 69 (1995).
- [17] A. B. Kolomeisky, G. M. Schütz, E. B. Kolomeisky, and J. P. Straley, *J. Phys. A: Math. Gen.* **31**, 6911 (1998).
- [18] V. Popkov and G. M. Schütz, *Europhys. Lett.* **48**, 257 (1999).
- [19] V. Popkov and I. Peschel, *Phys. Rev. E* **64**, 026126 (2001).
- [20] E. Pronina and A. B. Kolomeisky, *J. Phys. A: Math. Theor.* **40**, 2275 (2007).

- [21] J. Krug, *Braz. J. Phys.* **30**, 97 (2000).
- [22] M. R. Evans, D. P. Foster, C. Godrèche, and D. Mukamel, *Phys. Rev. Lett.* **74**, 208 (1995).
- [23] T. Kretz, A. Grünebohm, M. Kaufman, F. Mazur, and M. Schreckenberg, *J. Stat. Mech.* (2006) P10001.
- [24] W. O. Hancock, *Nat. Rev. Mol. Cell Biol.* **15**, 615 (2014).
- [25] V. Popkov, M. R. Evans, and D. Mukamel, *J. Phys. A: Math. Theor.* **41**, 432002 (2008).
- [26] E. Levine and R. Willmann, *J. Phys. A: Math. Gen.* **37**, 3333 (2004).
- [27] A. Jindal and A. K. Gupta, *Phys. Rev. E* **104**, 014138 (2021).
- [28] N. Sharma and A. Gupta, *J. Stat. Mech.* (2017) 043211.
- [29] B. Pal and A. K. Gupta, *J. Phys. A: Math. Theor.* **54**, 405002 (2021).
- [30] D. W. Erickson, G. Pruessner, B. Schmittmann, and R. K. Zia, *J. Phys. A: Math. Gen.* **38**, L659 (2005).
- [31] A. Jindal, A. B. Kolomeisky, and A. K. Gupta, *J. Stat. Mech.* (2020) 113202.
- [32] A. Jindal and A. K. Gupta, *Chaos Solitons Fractals* **152**, 111354 (2021).
- [33] A. K. Verma, N. Sharma, and A. K. Gupta, *Phys. Rev. E* **97**, 022105 (2018).
- [34] A. Gupta, B. Pal, and A. K. Gupta, *Phys. Rev. E* **107**, 034103 (2023).
- [35] R. Wang, M. Liu, and R. Jiang, *Phys. Rev. E* **77**, 051108 (2008).
- [36] N. C. Pesheva and J. G. Brankov, *BIOMATH* **1**, ID (2012).
- [37] N. Z. Bunzarova, N. Pesheva, and J. Brankov, *Physica A* **438**, 645 (2015).
- [38] I. Neri, N. Kern, and A. Parmeggiani, *Phys. Rev. Lett.* **107**, 068702 (2011).
- [39] I. Neri, N. Kern, and A. Parmeggiani, *New J. Phys.* **15**, 085005 (2013).
- [40] I. Neri, N. Kern, and A. Parmeggiani, *Phys. Rev. Lett.* **110**, 098102 (2013).
- [41] M. E. Fouladvand, Z. Sadjadi, and M. R. Shaebani, *Phys. Rev. E* **70**, 046132 (2004).
- [42] B. Ray and S. N. Bhattacharyya, *Phys. Rev. E* **73**, 036101 (2006).
- [43] H. Yamamoto, D. Yanagisawa, and K. Nishinari, *Phys. Rev. E* **108**, 044121 (2023).
- [44] N. C. Pesheva and J. G. Brankov, *Phys. Rev. E* **87**, 062116 (2013).
- [45] J. Brankov, N. Pesheva, and N. Bunzarova, *Phys. Rev. E* **69**, 066128 (2004).
- [46] L. S. Goldstein, *Proc. Natl. Acad. Sci. USA* **98**, 6999 (2001).
- [47] D. D. Hurd and W. M. Saxton, *Genetics* **144**, 1075 (1996).
- [48] D. Adams, B. Schmittmann, and R. Zia, *J. Stat. Mech.* (2008) P06009.
- [49] M. Ha and M. den Nijs, *Phys. Rev. E* **66**, 036118 (2002).
- [50] T. L. Blasius, N. Reed, B. M. Slepchenko, and K. J. Verhey, *PLoS ONE* **8**, e76081 (2013).
- [51] P. Greulich, L. Ciandrini, R. J. Allen, and M. C. Romano, *Phys. Rev. E* **85**, 011142 (2012).
- [52] L. J. Cook and R. Zia, *J. Stat. Mech.* (2009) P02012.
- [53] C. A. Brackley, L. Ciandrini, and M. C. Romano, *J. Stat. Mech.* (2012) P03002.
- [54] T. Banerjee and A. Basu, *Phys. Rev. Res.* **2**, 013025 (2020).